Highlights

- first description of the sequential order of authigenic mineral formation
- the secondary porosity forms the main contributor for the reservoir potential
- tight gas accumulation took place concomitant with densification of the reservoir

Graphical abstract

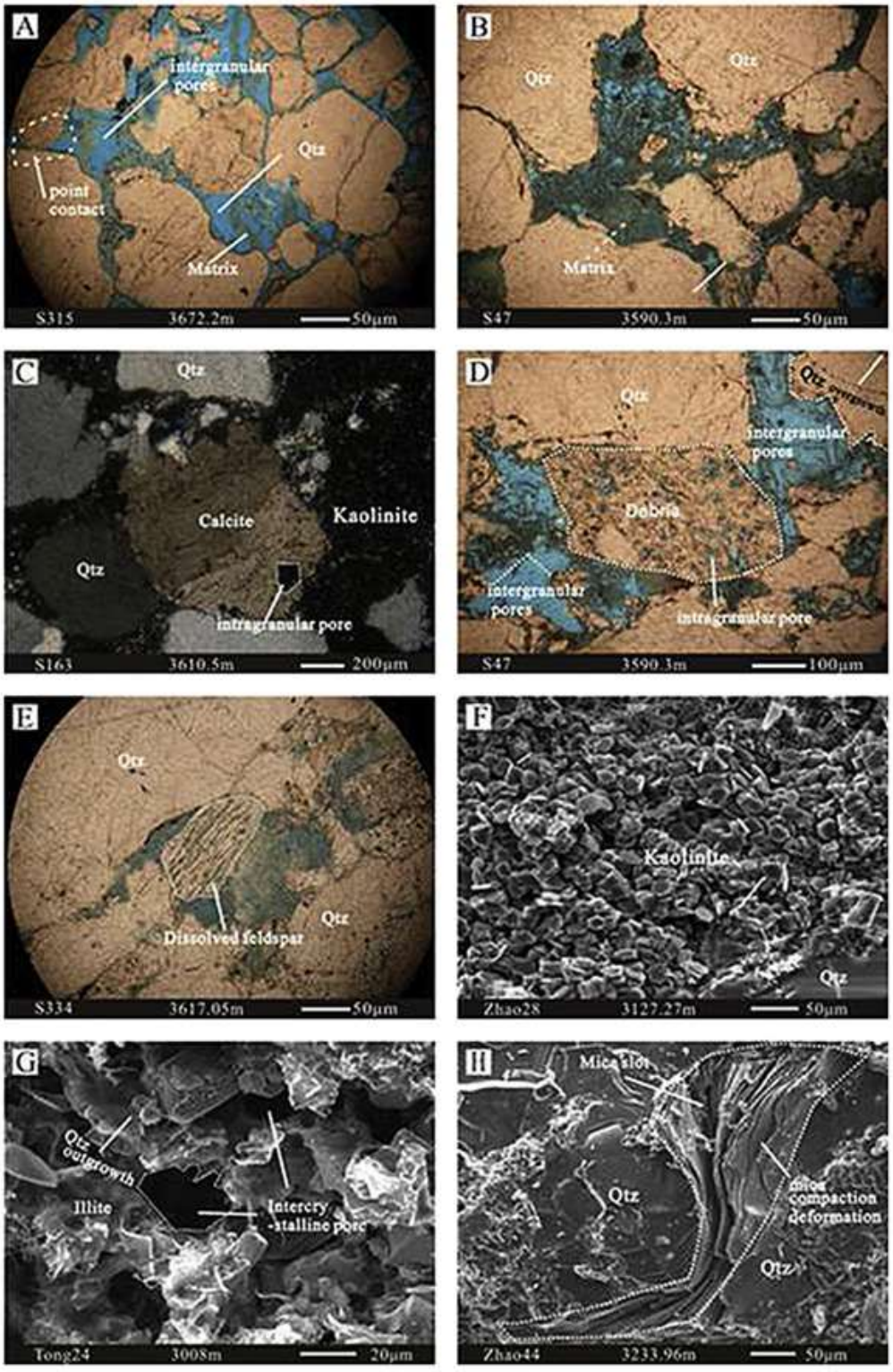

Cementation and porosity evolution of tight sandstone reservoirs in the Permian Sulige gas field, Ordos Basin (central China)

Aiping Fan[a,*], Renchao Yang[a, b,*], Nils Lenhardt[c], Meng Wang[a], Zuozhen Han[a], Jinbu Li[d], Yijun Li[d], Zhongjun Zhao[d]

[a] *College of Earth Science and Engineering, Shandong University of Science and Technology, Qingdao 266590, Shandong, China; e-mail: yang100808@126.com*
[b] *Laboratory for Marine Mineral Resources, Qingdao National Laboratory for Marine Science and Technology, Qingdao 266071, China; e-mail: yrc26@qq.com*
[c] *Department of Geology, University of Pretoria, Private Bag X20, 0028 Pretoria, South Africa*
[d] *Institute of exploration and development, Changqing Oilfield Company, Petrochina, Xi'an 710069, Shaanxi, China*

* Corresponding authors:
Aiping Fan; e-mail: xiaofan781026@sina.com
Renchao Yang; e-mail: yang100808@126.com

Abstract:

Tight sandstone gas reservoirs constitute an important type of unconventional gas resources and may be of crucial significance for clean energy in the world. However, the dynamics of densification and evolution of the low-porosity and low-permeability sandstone reservoirs are intensively debated in the literature. Recently, the question of sequence of reservoir densification and hydrocarbon accumulation has arisen. A typical tight sandstone reservoir in the Permian Sulige gas field in Central China provides an excellent case study to probe these questions. By using a variety of different methodologies such as scanning electron microscopy (SEM), X-ray diffraction (XRD), cathodoluminescence, fluid inclusion analysis and confocal Raman spectrometer analysis, we identified different authigenic minerals such as illite,

kaolinite, dickite, chlorite and smectite illitization coexisting with siliceous and calcitic cements. These authigenic minerals precipitated at different diagenetic stages, related to the changing conditions during compaction and lithification, and therefore, changed the porosities of the host rocks during each of these stages. The types of pores in the Sulige gas field are dominated by illite intercrystalline pores, kaolinite intercrystalline pores, matrix solution pores, and primary intergranular pores. The results of this study suggest that compaction and cementation are the reasons for the most distinct loss in porosity. On the other hand, kaolinite and illite preserve their intercrystalline pores, which could be identified as the main reserve space of the tight gas reservoirs. Therefore, the secondary porosity of the sandstone reservoirs forms the most important contributor to the gas reservoir potential in the Sulige gas field. In addition, it could be inferred that the tight gas accumulation took place during the densification of the reservoirs.

Key words: tight sandstone, gas reservoirs, diagenesis, authigenic mineral, Permian, Sulige gas field, Ordos basin

1. INTRODUCTION

The diagenesis of clastic rocks forms an important key factor related to the exploration and development of petroliferous basins (Fan et al., 2006, 2017; Li et al., 2008; Huang et al., 2009; Yang, H. et al., 2012; Yang and Liu, 2014; Yang, R. et al., 2014a). In addition, diagenesis and diagenetic processes play a decisive role in the formation and evolution of pores in clastic reservoirs. Diagenesis is a complex process that is controlled by numerous inter-related parameters, such as detrital

composition, depositional facies, climatic conditions, tectonic settings, and burial history, as well as the chemical composition and flow patterns of basin fluids (Stonecipher et al., 1984; Wilson and Stanton, 1994; Morad et al., 2000). For instance, the detrital composition is a main controlling factor for the reservoir properties of a clastic rock in terms that particles that can easily be deformed and react in a plastic manner or fine grain sizes are prone to dense compaction, thus leading to low porosities during diagenesis. Dissolution is a constructive factor in improving the properties of reservoirs during diagenesis. Dissolution is not only related to the corrosion capacity and active degree of underground fluids, but also to the amount of easily soluble components (such as carbonates and feldspars) contained in the rock itself and the diagenetic stage, pore connectivity, formation temperature, faults, and unconformity development of the rock. Diagenetic minerals form the record carriers of these diagenetic processes as they are closely related to the changes observed in the original detrital components (dissolvable grains, such as feldspars etc.) as well as the formation and destruction of pores. Therefore, the study of authigenic minerals during the different stages of diagenesis can be essential for a precise characterization of the reservoir quality.

The Sulige gas field, located in the central to north Ordos Basin, is the largest gas field in China (Yang, H. et al., 2012). Its annual gas production constitutes more than 30 billion cubic meters (Yang, H. et al., 2014). The first member of the lower Permian Shanxi Formation (P_1s_1) and the eighth member of the middle Permian Shihezi Formation (P_2h_8) in the Sulige gas field represent the main gas productive layers of the basin (Yang, R. et al., 2014a; Fan et al., 2017). Large-scale natural gas exploration in the Sulige gas field, belonging to the stratified constant volume gas

reservoirs of lithologic traps, started in 2000 (Fan et al., 2006; Li et al., 2008; Huang et al., 2009; Yang, H. et al., 2012).

Previous researchers have conducted extensive research on the sandstone reservoirs of the Sulige gas field (e.g., Fan et al., 2006; Li et al., 2008; Huang et al., 2009; Yang, H. et al., 2012; Yang, R. et al., 2014a; Fan et al., 2017). Some of these studies focused on the basic characteristics of various diagenetic features and processes (e.g., the strength of compaction, various types of cementation, and the type and extent of corrosion), highlighting the influence of different diagenetic processes on pore evolution and the physical reservoir properties (Li et al., 2008; Huang et al., 2009; Yang, H. et al., 2012; Yang, R. et al., 2014a; Fan et al., 2017). In case of the above mentioned formations of the Sulige gas field, it was proposed that the reservoir's densification took place from the Late Triassic to the Middle Jurassic, mainly due to compaction and siliceous cementation, and recording important information on the “pre-dense, post-reserve” time (Li et al., 2008; Yang, H. et al., 2012). In addition, high amounts of clay minerals and carbonate cements have been observed, that may have an immense effect on the reservoir quality (Yang, R. et al., 2014a; Fan et al., 2017). Despite the previous efforts, very few publications (Yang, H. et al., 2007; Yang, R. et al., 2014a; Fan et al., 2017) focused on the sources of the various diagenetic minerals, the diagenetic conditions and their controls on pores in the Sulige gas field. Therefore, the aims of this contribution are the following: 1) to investigate the origin and environmental conditions for the formation of diagenetic cements; 2) to ascertain the pore types and the origin of secondary porosity of sandstone reservoirs in the gas field; 3) to better understand the paragenetic sequence of the multiple cementation events and their influence on pore types and pore evolution, and 4) to shed light on the reason and time range of the reservoir

densification, i.e. whether the reservoir became dense after the first compaction or after the first accumulation.

2. GEOLOGICAL SETTING

2.1 Tectonic setting

The Ordos Basin is a polycyclic intracratonic basin that developed on the Archean crystalline basement. It is situated at the western part of the Sino-Korean Plate, as a walled basin (Carroll et al., 2010), which is bordered by the Yinshan, Luliang, Qinling, Liupan and Helan Mountains to the north, east, south, and west, respectively (Fig. 1) (Darby and Ritts, 2002; Xie and Heller, 2013; Yang, R. et al., 2014b, 2017). It has been intensively studied for its important resources of gas (Paleozoic) (Yang, R. et al., 2014b), oil (Mesozoic) (Zhang et al., 2013; Xie and Heller, 2013; Yang, R. et al., 2014b, 2017a; Wang et al., 2017), coal (Paleozoic and Mesozoic), uranium (Mesozoic) (Mao et al., 2014), and metal deposits (Cao et al., 2017). In addition, its provenance of clastic material and regional tectonic settings at different geological times have been documented in literature (Li, X. et al., 2011, 2014, 2015, 2017; Qiu et al., 2014; Liu et al., 2015; Song et al., 2016; Du et al., 2017).

According to the present structural forms, the basin can be divided into six first-class structural units (Fig. 1), such as the Yimeng uplift, the Weibei flexural belt, the Jinxi flexural belt, the Yishan slope, the Tianhuan depression and the western marginal thrust fault belt (Min et al., 2000; Yang, R. et al., in press). The Sulige gas field is located in the north-central part of the Yishan slope (Ordos basin), a west inclined structural unit (Fig. 1).

2.2 Sedimentary and stratigraphic setting

The basin is characterized by marine sedimentation from the Proterozoic to the Middle Ordovician (Yang, R. et al., in press). After a hiatus spanning from the Late Ordovician to the Early Carboniferous, sedimentation was prepresented by an alternating deposition of terrestrial and epeiric sea sediments during the Late Carboniferous until the Early Permian. This time, distinctive for its coal-bearing formations within the basin, was characterized by warm and humid climatic conditions, which were favorable for the formation of quartz sandstone with high compositional maturity (Lewis, 1989). From the Middle to the Late Permian, sedimentation took place in a fluvial-deltaic to lacustrine environment (Yang, R. et al., 2014a). Finally, the end of deposition within the Ordos Basin was characterized by lacustrine sedimentation during Mesozoic and Cenozoic times (Yang, R. et al., 2014b, 2017a, b; Fan et al., 2017, 2018).

The Sulige gas field is characterized by Paleozoic sediments, i.e. the Carboniferous Benxi and Taiyuan formations, and the Permian Shanxi, the Lower Shihezi formations, the Upper Shihezi formations and Shiqianfeng formations (Fig. 2A). The base of the Upper Carboniferous Benxi Fm. (35-45 m thickness) is formed by ferralic rocks, directly overlying the Majiagou Formation (dolomites, limestones, dolomitic gypsum and gypsum). The top of the Benxi Fm. is characterized by the lower coal seams (coal seams $8^{\#}$) of the basin. The strata of the Taiyuan Fm. are continuously deposited on top of the Benxi Fm., with the Miaogou limestone forming the lower and the base of the Beichagou sandstone forming the upper boundary of the formation. The Taiyuan Fm. is widely distributed in the area with thicknesses spanning from 25-40 meters and thinning from east to west.

The Permian succession is divided into three series. The Shanxi Fm. (Lower Permian) on top of the Taiyuan Fm. starts Beichagou sandstone. Its upper boundary is

formed by the base of the “Luotuobozi sandstone”. The whole formation reaches thicknesses of 90-110 m and exhibits a slight thinning towards the west. According to the sedimentary sequence and lithological association, the Shanxi Fm. can be divided from base to top into two members, the 2nd member (P_1s_2) and the 1st member (P_1s_1). The thickness of P_1s_2 is 45-60 m. The member consists of a set of quartz sandstones with thin intercalated layers of siltstone, mudstone and coal seams. The thickness of P_1s_1 is 40-50 m. This member is mainly composed of grayish-white, fine-medium grained sandstone that is intercalated with carbonaceous and dark gray mudstones.

The Middle Permian is characterized by the Lower and Upper Shihezi formations. The Luotuobozi sandstone forms the basal boundary of the Lower Shihezi Fm., the “Taohua mudstone” its top. The lithology of the Lower Shihezi Fm. (120-160 m in thickness) is represented by gray, gravelly coarse sandstones, grayish-white medium coarse grained sandstone, gray-green lithic quartz sandstone and variegated mudstones. According to its sedimentary cycle, the formation can be divided into four gas-producing members from base to top: P_2h_8, P_2h_7, P_2h_6, and P_2h_5. The lithology of P_2h_8 (80-100 m in thickness), the most important gas producing layer in the Sulige gas field, is predominantly composed of coarse- to medium-grained sandstone, and subordinate fine sandstone and siltstone.

The Upper Shihezi Fm. (140-160 m in thickness) is mainly composed of red and sandy mudstones, with thin layers of sand- and siltstone. The overlying Shiqianfeng Fm. (Upper Permian; >200 in thickness) is mainly composed of reddish gravelly sandstones and sandy mudstones that are locally interbedded with calcareous marl nodules. The main gas-bearing strata in the Sulige area are P_1s_1 and P_2h_8, which also form the main focus of this contribution.

2.3 Gas reservoir geology

The source rocks of the Sulige gas field are mainly the coal seams and carbon-rich mudstones of the Carboniferous Benxi and Taiyuan formations and the Permian Shanxi Formation (Fig. 2A). From the perspective of the thermal evolution of the source rocks, the R_0 values of these rocks are reach to 1.6%. The mature stage with peak gas generation and extensive hydrocarbon generation was reached during the Late Jurassic-Early Cretaceous (Min et al., 2000; Wang et al., 2011; Yang and Liu, 2014).

The reservoir rocks that form the focus of this contribution (P_1s_1 and P_2h_8) are mainly composed of sandstones and are situated directly on top of each other. They are considered a broad-based source of a combination of lower generation and upper reservoir (Fig. 3) with a contact area of up to 10×10^4 km^2.

The mudstones and silty mudstones of the Lower Shihezi Fm. Form the direct cap rocks. Locally, the mudstones of the Upper Shihezi and Shiqianfeng formations may also form additional cap rocks.

The average burial depth of the gas reservoir is ca. 2998 m. The geothermal gradient is 3.03°C/100 m. The formation pressure is between 24.19-27.80 MPa and the average pressure coefficient is 0.86 (Yang, H. et al., 2014). The reservoir is described as a typical low-pressure gas reservoir (Yang, H. et al., 2014; Yang, R. et al., 2014a). It has strong reservoir heterogeneity, many gas-bearing reservoirs, large area, low reserve abundance and multiple pressure systems (Yang, H. et al., 2014). The burial history curve (Fig. 4) shows that, four unbalanced uplift and erosion events occurred in the Sulige area that are marked by an unconformity at the Triassic/ Jurassic boundary (Indosinian, ~200 Ma), the early Yanshanian movement, (~175 Ma), the middle Yanshanian movement (~145 Ma) and the late Yanshanian

movement (~65 Ma) since the Mesozoic. The first three periods of erosional events were relatively weak with small amounts of erosion (Table 1). The basin was rapidly uplifted by the influence of the Yanshanian movement and the subsequent Himalayan movement since the end of the early Cretaceous. The average denudation thickness of the basin is 509.6 m (Zhang, W., 2009). The depth of the source rock is shallow and the temperature of the formation is greatly reduced, while the thermal evolution and hydrocarbon generation of the source rock gradually weaken until it stopped.

3. MATERIALS AND METHODS

The lithology and petrography of the P_1s_1 and P_2h_8 sandstone samples from the Sulige gas field were studied by polarized light microscopy, scanning electron microscopy (SEM), X-ray diffraction (XRD), cathodoluminescence, fluid inclusion analysis and confocal Raman spectrometer analysis. 310 drill core samples were used for macroscopic description. Of these, 220 thin sections were produced for further in-depth studies. Blue resin was used for thin sections in order to make statistical analysis more convenient and allow an easier description of pore types, their occurrence, distribution characteristics and contact relationships between the matrix particles. In addition, a solution of potassium ferricyanide and alizarin red was used on the thin sections for 20 minutes in order to color the carbonate minerals within the sandstones. As a result to the chemical reaction, pure calcite turns red, which may be a purplish red in case the calcite contains iron. If iron-containing dolomite reacts with the solution, its color turns bright blue.

SEM and cathodoluminescence analyses were combined to further describe the occurrence of different diagenetic minerals, their relationship towards each other, and the pore characteristics of the sampled sandstones. A SYKY-2800B electron

microscope was used for SEM analysis. The performance indices of the instrument are the following: acceleration voltage (0.1-30 Kv), magnification (15-250,000×), resolution better than 4.5 nm; test conditions: voltage (20 Kv), vacuum degree (0.05 mbar). A RELION III CL was used for cathodoluminescence to recognize autogenetic minerals. The performance indices of the instrument are the following: acceleration voltage (0-20 Kv), magnification (20-250×); test conditions: voltage (~15 Kv), current (~1.2 mA), and vacuum degree (~0.05 mbar).

XRD was performed using an X'Pert-Pro powder diffractometer (manufactured by Panalytical in the Netherlands) under the following conditions: voltage (40 Kv), current (40 mA), and diffraction angle (5-60°).

In addition, a Nikon COOLPIX4500 microscope was used to observe the color, shape, size and occurrence of fluid inclusions under the conditions of transmission light and fluorescence to determine the phase states and distribution characteristics of fluid inclusions. Fluid inclusion analysis may be of benefit to reconstruct temperature, pressure, salinity and chemical component of paleofluid, and thus to infer diagenesis information. Fluid inclusions trapped in autogenetic minerals, such as quartz overgrowth and carbonate cements, were measured by the instrument. The instrument for measuring the temperature of fluid inclusions was a THMS-600 (Linkham, UK) micro hot and cold stage (-196~600°C) with a test precision of ±1°C. Laser Raman measurement of seven fluid inclusions was carried out at the State key Laboratory of Deposit Geochemistry at the Institute of Geochemistry, Chinese Academy of Sciences. The instrument was a British Renishaw in Via Reflex visible microscopic confocal Raman spectrometer with a laser source of 514.5 nm, and a spectral resolution of 0.6 cm^{-1}.

4. RESULTS

4.1 Sandstone Lithologies

Observations on drill core material show that the main reservoir lithologies of the P_2h_8 of the Sulige gas field are grayish gravelly sandstone, coarse sandstone, medium sandstone, greenish-gray medium to fine sandstone. The main reservoir lithologies of the P_1s_1 are greenish-gray gravelly sandstone, coarse sandstone, very light gray medium-coarse sandstone, and light gray fine sandstone (Fig. 5). The lithofacies of the sandstone reservoir of the P_2h_8 and P_1s_1 members has been documented in detail by Yang, R. et al. (2014a).

In general, the sandstone within the study area can be described as medium mature. According to the analysis of 220 thin sections, the average value of the matrix content is 9.2%. The type of reservoir rock is mainly litharenite, followed by quartz arenite and greywacke (Fig. 6). The degree of roundness of the grains is predominantly angular to subangular with small amounts of sub-rounded grains. The sphericity of the grains is dominated by medium to subspherical grains. The main particle size range is 0.2-1.6 mm with an average of 0.56 mm. The grains predominantly exhibit long contacts. However, subordinately some point and concavo-convex contacts can be observed as well. The content of quartz is between 40-85% (based on point counting of 400 grains for each thin section), with an average of 64.2%, including single- crystal quartz and polycrystalline quartz. The content of feldspar is very small (0-7.14%; 0.36% on average) with most crystals completely kaolinized. The amount of lithic fragments ranges between 0-45% with an average of 16%. Among them, with up to 36% (10.9% on average), the metamorphic rock fragments (granulites, schists, slate, etc.) have the highest content. These are followed by igneous rock fragments (granite, rhyolite and andesite) with contents up to 15%,

and an average content of 3.9%. The content of sedimentary rocks among the lithic fragments is less than 6%, with an average of 0.3%. These fragments can usually be characterized as mudstone, argillaceous siltstone, and siltstone. The cement types are related to the grain contact relationship and is predominantly porous cement (linear supported grains), followed by basal cementation (matrix-supported grains) and subordinate contact cementation (point by point supported grains).

The existence of minor volcaniclastic material within the sandstones described above is an important characteristic of the sandstone composition in the Sulige gas field (Yang, H., et al., 2007). The volcanic debris was close to the source area, implying a relatively short time of in-situ weathering and absence of long-distance transport. As a result, some chemical properties of unstable and soluble volcanic components could remain without complete weathering (Yang, Y., 2008). The volcaniclastic sediments are characterized by lithic fragments set in a fine-grained matrix of volcanic ash. The types of lithic fragments include a whole range of compositions including basalts, andesites and rhyolitic tuff fragments. The volcanic ash matrix exhibits dark brown Ti-Fe-rich, femic, and intermediate-felsic vitric fragments. Due to the wide range of different compositions within these deposits, it can be assumed that a reworking of the material took place before its final deposition. Nevertheless, the volcaniclastic rocks form an important contributor to the formation of the reservoir.

4.2 Authigenic Mineralogy

The average value of cement content within the samples is 15.6%. Among the different types of cement the clay mineral content (on average 9.8%) appears to be most important. The clay minerals are followed by calcite cement (on average 5.08%),

and siliceous cement (on average 0.72%). In the following sections, the cement types are described in detail.

4.2.1 Kaolinite and Dickite

Kaolinite is the most widely distributed diagenetic mineral within the analyzed samples with an average content of 6.83% in the P_1s_1 and 5.89% in the P_2h_8 samples, mostly filling intergranular pores. The results of casting and scanning electron microscopy show that the intergranular pores are commonly filled with up to 60% of kaolinite. This cement type is mostly developed in the litharenites, greywackes and quartz arenites. Generally it can be seen that the larger the thickness of the sandstone is, the larger the kaolinite crystals are. Under SEM, the kaolinite exhibits a pseudo-hexagonal morphology. Aggregates of kaolinite are sheet- or worm-like. No extrusion deformation is visible. Occasionally, feldspar and volcanic rock debris residues are found coexisting with authigenic kaolinite and are engulfed by quartz cement. As a result of shallow burial and limited compaction, kaolinized micas have expanded into adjacent pore spaces. Under the microscope, the relationship between kaolinite and its source minerals can clearly be identified (Fig. 7). Kaolinite always occurs around plagioclase (Fig. 7A), fills in dissolution pores of K-feldspar (Fig. 7B) and plagioclase (Fig. 7C), or in adjacent pores around dissolved plagioclase (Fig. 7D) and rock debris (Figs. 7E and F). Especially plagioclase and K-feldspar, either as single crystals or within rock debris, have undergone extensive dissolution to form kaolinite under apparently acidic conditions.

Dickite and kaolinite have the same chemical composition but different crystal structures for which reason detailed microscopic observations or XRD measurements are necessary to distinguish the two (Fig. 8). Within the samples, the kaolinite occurs

as long (up to 30 μm) and thin (<2 μm) crystals whereas the dickite appears to be as rather blocky (2-10 μm thick and 5-15 μm across) (also see Morad & De Ros, 1994). Generally, kaolinite crystals have etched surfaces owing to partial dissolution, whereas dickite crystals exhibits rather smooth surfaces (c.f., Khalifa et al., 2008, 2012). SEM observations of the dickite show that the monomer form is hexagonal tabular and the slice thick (Fig. 9A).

4.2.2 Illite

The analyzed samples generally show high contents of illite, with 3.1% in the P_1s_1 and 3.34% in the P_2h_8 samples. The illite is mainly developed in litharenite, but it is rare in quartz arenite. Most of the observed illites, filling the pore spaces of the sandstones, exhibit good crystal shapes. The illite is mainly produced in three ways: 1) One type is characterized by vertical growth on the surface of detrital grains, forming an envelope around the grains (an isopachous cement fabric). This type could only be observed in Well S315 (see Fig. 8). It presumably formed at an early stage and results from conversion from matrix, inferred from its occurrence mentioned above. 2) The second type was produced in the form of reticulate illite aggregates in the intergranular pores. Most of the reticulated illite is produced in detrital feldspar or rock fragments that are completely or partially dissolved, and appears as a group of nearly parallel arranged illite aggregates. 3) The third type of illite cement fills the space between grains (Fig. 10a). Among the three types of illite, the latter type is the most abundant in the samples. There is no obvious reticulated structure. The edges of the illite crystals may be curled, developing from lamellar forms to silk threads. Aggregates may retain a semi-cellular structure. In addition, some illites show intergrowth textures with kaolinites, which are mostly flaky or filamentous crystals,

and preserving to varying degrees the primitive structure of the sheet-like kaolinite aggregates.

4.2.3 Chlorite

In the sandstones of this area, with 0.74% in the P_2h_8 and 0.57% in the P_1s_1 samples, chlorite cement appears to be relatively rare. The cement is characterized by chlorite rings (Fig. 10b), chlorite altered from biotite (Fig. 10c), and chlorite linings around quartz grains (Fig. 10d). The chlorite rings that can be found either enveloping entire particles continuously or discontinously exhibit widths between 1 and 5 μm. Furthermore, they can also be observed at the detrital particle contact points. The thickness of the pore lining chlorite varies from 5-10 μm. The difference to the above mentioned chlorite rings is that the chlorite crystals are relatively large, appear in the shape of pectinate shells, and are arranged continuously along the clay ring boundary, perpendicular to grain surface. The size of chlorite increases from the surface of the particle to the center of the pore, and idiomorphic chlorite becomes more and more. Under plane-polarized light, it can be seen that the biotite has altered to chlorite and it shows that the color of biotite becomes light green. The cleavage of biotite is still preserved, and the interference color of biotite decreases under orthogonal polarized lights, showing gray and black colors.

4.2.4 Carbonate cement

Carbonate cements are sensitive to acid - alkali anomalies of the pore fluid and easy to dissolve, precipitate, re-dissolve and re-precipitate. Therefore, carbonate cements are good mineral indicators for pH changes of the diagenetic environment (Wang, Q., et al., 2010). Within the analyzed samples, the carbonate cement is mainly

calcite, with contents up of to 5.08%. Three types of calcite cements could be observed within this study: 1) calcite fill in intergranular pores, occupying the central part of the pore. Commonly more than one type of cement can be found within these pores with a ring of clay minerals along the pore walls, a quartz cement growing towards the center of the pore and finally the calcite cement itself forming the center of the pore; 2) sparry calcite binds multiple grains, forming inlaid crystals cement, in which residual pores are difficult to preserve; 3) calcite replaces kaolinite, illite and siliceous cementation.

The distribution of the calcite cement suggests that it is generally formed at a late cementation stage, i.e. after the formation of the clay minerals and silica cementation, and may be responsible for immensely reducing the reservoir quality by sealing the pore spaces.

4.2.5 Siliceous cement

Under the microscope and SEM, two types of siliceous cements could be observed within the samples, i.e. quartz overgrowth and quartz microcrystals (outgrowth). The quartz overgrowth is mainly developed in the sampled arenites. Its content is up to 4%, with an average of 0.72% by volume. It is usually distributed around the quartz grains. Some extensions show a clear “dirty line” between the original clastic quartz grain and the cement (very thin discontinuous clay rings or fluid inclusions are separated). Straight edges of quartz overgrowth exist around the clastic quartz grains. The straight edges of the authigenic quartz overgrowth in thin section imply the existence of free pore space during the growth of authigenic quartz. In the analyzed samples, the width of quartz overgrowth varies from 5-50 μm. Most of the overgrowth developed in one phase. Nevertheless, locally, up to three phases of

quartz overgrowth were observed. The shapes of quartz overgrowth are determined by two main factors. One is that the quartz growth is restricted by the surrounding space. The other factor is the existence or absence of dissolution around the edge of quartz in an alkaline environment at a late diagenetic stage (Fig. 11A). SEM observations show that quartz overgrowth is mostly associated with kaolinite and consists of the same optical orientation with quartz grains, plugging a part of the pore.

Quartz microcrystals or outgrowths are observed in litharenites. They may appear as separated/single crystals or as crystal aggregates. The crystals grow perpendicular to clastic particles or on the base of clay mineral particles with complete crystal planes. Furthermore, quartz outgrowths occur on grains coated extensively by filamentous and/or fibrous illite (Fig. 11B). Quartz outgrowths (20-30 mm thick) do not occur around quartz grains that are coated extensively by illite (Fig. 11B) or by rare micro-quartz (c.f. Khalifa et al., 2012).

4.3 Fluid inclusion microthermometry of cements

The fluid inclusions studied for this contribution are limited to the secondary fluid inclusions that are closely related to the fluid evolution of the sedimentary basin, and are related to quartz doubling, quartz microcracks and carbonate cement. According to the physical phase and composition of the inclusions at room temperature, the secondary inclusions of the samples are divided into brine inclusions, CO_2 inclusions, and hydrocarbon inclusions.

4.3.1 Temperature measurement of fluid inclusions

4.3.2.1 Homogeneous temperature and salinity

The number of two-phase brine inclusions developed at quartz overgrowths is relatively small. The diameters of the inclusions are generally between 2-3.5 μm. The gas-liquid ratios are between 5-10%. Furthermore, they are colorless and hyaline under single polarized light. Due to the small size of the inclusions, the initial melting temperatures could not be accurately observed, and only the data of uniform temperature and salinity were obtained. The homogeneous temperatures are mainly distributed between 79.4-148.4°C. Calculated salinities are between 3.55-1.25 wt.% within an average value of 6.60 wt.%.

Only two-phase brine inclusions could be observed in carbonate cements, exhibiting diameters between 3.5 and 6 μm. Some elongated inclusions show diameters between 15 and 20 μm. The gas-liquid ratios of these inclusions range between 4-6%. The bubble walls appear thick. The bubbles are not active with elongated and irregular shapes and yellowish colors under the single polarized light. The carbonate cement itself is affected by light refraction and only homogenous temperature data could be obtained. The range of homogenous temperatures is between 170.3-188.6°C with an average of 179.8°C (Fig. 12).

The number of two-phase brine inclusions in the quartz microcracks is numerous. The diameters of these inclusions range between 3-20 μm. Gas-liquid ratios are between 5 and 30%. The shape of the inclusions is mainly elliptical, elongated and irregular. Furthermore, they appear colorless to light pink under plane polarized light. Their homogenization temperatures range between 63-155°C with a concentration between 85-155°C (> 60% of the analyzed samples), which is basically the same as the temperature measured in the quartz overgrowths. This indicates that this temperature range is the active phase of the fluid, and the water-rock activity is intense, because most of fluid inclusions were formed in that temperature range.

According to the initial melting temperature (ranges of -62.7 to -33.4°C) of fluid inclusions in the quartz microcracks, the water-salt system of the fluid inclusions in the P_1s_1 and P_2h_8 samples is not a single H_2O-NaCl system. Instead, there are multiple fluid systems coexisting with each other, such as of H_2O-NaCl-$MgCl_2$ type, H_2O-$CaCl_2$ type, H_2O-KCl-$CaCl_2$ type, H_2O-$MgCl_2$-$CaCl_2$ type and H_2O-NaCl-$CaCl_2$ type. The salinity of fluid inclusions is 3.39-22.38 wt% with an average value of 12.40 wt.%. The salinity value of the study area is high, and there is no relation between salinity and homogenization temperature in the study area, indicating that the formation of fluid inclusions took place within a closed diagenetic system with restricted fluid activity between the strata. The salinity of water is mainly controlled by the diagenetic microenvironment.

4.4 Reservoir pore types and petrophysical properties

The average porosity of the sampled reservoir rocks is 9.1%, the average permeability 0.49 mD (Table 2), typical for low porosity and low permeability reservoirs. However, the average values of porosity and permeability cannot fully represent the physical characteristics of the reservoir because some sandstones have very poor physical properties while others exhibit relatively high values. The surface pore space of the thin sections in the study area varies from 0~15%, predominantly ranging between 2~5%, with an average of 3.69 in the P_2h_8 and 3.20% in the P_1s_1, which reflect low porosity of the sandstone reservoir in the Sulige gas field.

The pores within the samples for this contribution include primary and secondary pores. The primary pores account for 12.26% of the total pores and include primary intergranular and intragranular pores. The main pore types that could be observed, however, are secondary pores, accounting for 87.74% of the total pores. These include

dissolved pores (heterogeneous dissolved pores, calcite dissolved pores, lithic dissolved pores, and feldspar dissolved pores), accounting for 25.18% of the total observed pores. Interstitial intercrystalline pores (kaolinite intercrystalline pores and illite intercrystalline pores) account for 59.33% of the total pores, and mica hydration pores and microfractures account for 3.23% of the total pores, respectively (Figs. 14 and 15). The heterogeneity of the sandstone lithology (grain size or sorting) have a great influence on the surface porosity. Generally speaking, the larger grain size and the lower the heterogeneity of the sandstone lithology, the higher the surface porosity. If the heterogeneity exceeds 20%, the reservoir can be considered as tight.

The results show that the initial porosities of the P_2h_8 and the P_1s_1 members were 35.5% and 39.8%, respectively. The reduced porosities caused by compaction are 24.3% and 25.1%, respectively. The residual porosities are 11.2% and 14.7%. The total volume reduction rate before and after the dissolution of calcium feldspar and the formation of kaolinite is 1.26%, while the chlorite cementation only resulted in 0.65% reduction of pore volume, which shows that the porosity of the reservoir has decreased but it cannot be considered tight.

5. DISCUSSION

5.1 Sequential order of cement mineral formation

The sequential order of secondary mineral (cement) formation within the analyzed sandstones or paragenetic sequence could be reconstructed on the basis of textural and contact relationships between primary and secondary minerals (Yang, R., et al., 2014a). The chlorite ring edges can usually be found directly adjacent to the sedimentary grains. In addition, chlorite can be found occurring at the contact points of sedimentary grains and in the curved cleavages of biotite with the same orientation

(Fig. 10c). This implies that the pore spaces at the time of chlorite precipitation were still sufficiently wide, indicating that the formation of these minerals must have occurred before the compaction of the sediment. On the other hand, the chlorite ring peripheries are usually observed together with a large amount of kaolinite, a fact that may indicate that the formation of kaolinite took place later than the development of the chlorite ring edges. The pore lining chlorite grew in a ctenoid shape on the chlorite film and is absent at particle contact points, indicating that the pore lining chlorite began to form after the stage of compaction.

Kaolinite is engulfed by quartz overgrowth and quartz outgrowth, demonstrating that the formation of kaolinite took place earlier than quartz overgrowth and outgrowth. The edge of kaolinite mineralization is commonly illitized, which shows that the kaolinite formed earlier than the illite cement. The accumulation patterns of kaolinite varies from compacted to loose within the samples rocks. The accumulation patterns of kaolinite reflects the effect of compaction. The compacted accumulation indicates much compaction, while the loose accumulation implies less compaction. This may be an indication that the formation of kaolinite took place over a longer time, possibly more than one diagenetic stage during the process of compaction of the sandstones.

The wide range of homogenization temperatures of the brine inclusions in the quartz overgrowth demonstrates that the formation of the latter took a significant amount of time. This temperature range is conducive to the preservation of organic acids (Huang et al., 2009) and the formation of feldspar dissolution and quartz enlargement. Traces of hydrocarbon may be retained in the feldspar dissolved pores (Fig. 7). Therefore, it can be assumed that oil and gas charging took place after the

dissolution of feldspar. Feldspar dissolution mainly forms quartz enhanced and authigenic kaolinite by-products **(**Wei et al., 2011**).**

The observed quartz outgrowth wraps the chlorite linings, indicating that quartz outgrowth formation certainly took place after the development of the chlorite linings. Further evidence for a late stage formation of the quartz outgrowth can be seen in intergranular pores that had initially been filled by illite and where the former either occupied the remaining pore space in between illite crystals or grew on top of the illite. On the other hand, the quartz outgrowth may also be cut by illite during the growth process, which shows that the diagenetic environment may have been relatively complex in the temperature range of 79.4 - 148.4°C and, that quartz cement and illite may have alternately grown. Finally, the residual intergranular pore space was filled with a late calcite cement (in forms of meso-fine or xenotopic crystals, sometimes in the form of embedded cementation with smaller 'floating' particles in a bigger calcite crystal). The late stage of calcite replaces the edges of illite, chlorite and quartz overgrowth in a zigzagged shape.

5.2 Cement formation processes

5.2.1 The source of kaolinite

The formation of authigenic kaolinite is often related to the dissolution of aluminosilicates such as plagioclase, K-feldspar, etc. (Surdam, 1984; Brantley and Stillings, 1996; Wilkinson et al., 2001, 2003; Shaw, 2003). Kaolinite precipitation requires low pH and low ion concentration in water (Hammer et al., 2010)**.** Feldspar appears to be relatively scarce in thin sections under a normal polarizing microscope. However, using a cathodeluminescence microscope reveals the existence of K-feldspar, albite and plagioclase. This reflects that a large amount of feldspar may have

been deposited but was widely dissolved and reduced during the various diagenetic stages. Initially, the sandstone of the Shihezi Fm. was deposited in a fluvial and delta environment in a warm and humid climate (Lewis, 1989). The sandstone is characterized by a large-scale contact with the underlying coal seams and carbonaceous mudstones, the source rock for the hydrocarbons within the basin. Therefore, the sandstone was not isolated during burial and diagenesis but sustained a close relationship to the evolution of organic matter of the source rocks. Due to the high amount of organic acid produced during the decay of organic matter within these source rocks (Lewis, 1989), the syn-genetic environment can be assumed to have been relatively acidic. Furthermore, with the increase of vitrinite reflectance of the coal-based organic matter, additional CO_2 was released into the pore fluids, forming carbonic acid. These acidic pore fluids then reacted with the aluminosilicates in the overlying sandstones, causing the formation of kaolinite. The presence of dickite can be explained by partial or total transformation of kaolinite due to progressive burial of the host sediment to depths greater than 2 km and burial temperatures exceeding 70°C (Ehrenberg et al., 1989, 1993, 2001). The burial history curve (Fig. 4) in this area shows that the maximum depth of this area is 3,100 m with burial temperatures as high as 200°C, certainly providing the conditions for the conversion of kaolinite to dickite.

5.2.2 The source of illite

Illite is usually not generated during the early diagenetic environment. Instead, it commonly forms the main diagenetic clay mineral during the middle diagenetic stage (Sanjuan et al., 2003). In this stage, illite is formed by alteration of pre-stage clay minerals (e.g., smectite, kaolinite), clastic feldspar and lithic fragments (Meng et al.,

2011). The presence of various textural habits of illite (fibrous, platelet, honey-comb, mat and bacteria-like) suggests various controlling parameters and formation processes (Abouessa and Morad, 2009). Honeycomb-like illite most likely forms through the transformation of authigenic smectite (c.f., Worden and Morad, 2003a, 2003b, 2009), from which we infer that the semi-honeycomb illite in this area may originate from pre-existing montmorillonite. The reticular illite, which occurs in all or at least a part of the dissolved clastic feldspar or lithic debris, as well as the illite associated with kaolinite (Worden et al., 1998; Worden and Morad, 2003a), reflects the transformation balance of feldspar dissolution and illite and kaolinite formation during the diagenetic evolution (see next section).

5.2.3 Transformation balance between kaolinite and illite

Thermodynamic calculations (Huang, et al., 2009; Wei et al., 2011) show that the standard Gibbs free energy increments for the formation of kaolinite by three feldspars in an acidic medium environment are all less than 0. However, anorthite has the lowest standard Gibbs free energy compared to albite and K-feldspar ($\Delta G\Theta$). The energy varies from -297.49 to -217.43 KJ/mol, and the Gibbs free energy increases with increasing temperature, which indicates that kaolinization can occur at lower temperatures, and the effect of the diagenetic environment on the reaction is neglectable. It should be noted that there is no additional source of K^+ in the formation fluids in the area. The diagenetic system is open to semi-open so that kaolinite is formed instead of illite from the reaction of anorthite and acid. Whereas, reaction of K-feldspar and acid is exactly opposite to that of anorthite. Here, the standard Gibbs free energy decreases with increasing temperature, which indicates that K-feldspar is easy to dissolve at higher temperatures. In addition, K-feldspar

dissolution is usually controlled by the kinetics of dissolution and transport rates (Stroker et al., 2013). The breakdown of K-feldspar, observed in sedimentary basins, occurs in the approximate temperature interval of 100-120°C (Harris, 1992; Milliken et al., 1989; Boles and Franks, 1979) unless it is limited by high activity of K^+ or SiO_2 (Wilkinson et al., 2001). As a result, calcium feldspar dissolves shortly after deposition, resulting in kaolinite and Ca^{2+} release, and no discharge of SiO_2. The dissolution of K-feldspar occurs much later and is more complicated as it can produce either kaolinite or illite, depending on the $\alpha(K^+)/\alpha(H^+)$ ratio of pore fluid. We observed few of illite generated from feldspar but a lot of kaolinite related to feldspar in thin section.

Most K-feldspar formed kaolinite for two possible reasons: 1) the temperature range (100-120°C) during the dissolution of K-feldspar corresponds to the most acidic stage of organic matter evolution. Therefore, the concentration of H^+ ions in the diagenetic system is high; 2) the K^+ ion concentration of the sandstone pore fluid is low. This is related to the fact that during dissolution of K-feldspar, K^+ ions are first released into the pore fluid and thereafter either transported away or adsorbed by other minerals, resulting in a low concentration of K^+ ions in the water. As mentioned above, the blocking property of the diagenetic system is strong, and the released K^+ ions are difficult to be moved out of the system, leading to widespread transformation of montmorillonite to illite in this area. The results show that the conversion temperature of montmorillonite to illite is between 90 to 130°C (Morad et al., 1990, 2000; Ehrenberg, 1993; Morad and De Ros, 1994). This is a spontaneous reaction with low energy consumption and an important potassium consumption reaction, which can explain that K-feldspar forms kaolinite rather than illite at 100-120°C.

Geochemical simulations show that there is a threshold of 120-140°C for kaolinite illitization. Below this threshold, due to the low reaction rate, kaolinite illitization is not significant (Storvoll et al., 2002). Above this threshold, the dissolution of kaolinite, K-feldspar, and polysilicon muscovite becomes active, and the precipitation of illite occurs (Bross et al., 2003). Moreover, kinetics simulations show that the participation of organic matter from mudstone strata has no material effect on the reaction (Berger et al., 1997). As a result, when the diagenetic temperature exceeds 130°C, the organic acids in the pore fluids will gradually decrease, the conversion of montmorillonite to illite will stop, and instead kaolinite illitization will commence. The ratio of K-feldspar to kaolinite in a rock controls the dissolution of feldspar and the quantitative relationship among the K-feldspar, kaolinite and illite in the dissolution product. There is only part of kaolinite has illitization, it shows that the content of potassium feldspar is less than that of kaolinite, which is not enough to make most kaolinite illitization. K-feldspar is almost completely dissolved. Therefore, the sedimentary grains of the sandstones in the Sulige gas field are predominantly quartz and lithic particles. Associated authigenic clay minerals are kaolinite and illite.

5.2.4 Siliceous cement

The source of silica in quartz cementation has been discussed by a variety of authors in the past (McBride, 1989; Dutton and Diggs, 1990; Weber and Ricken, 2005). Stylolites and micro-stylolites for instance have been recognized as sources of quartz cement (Bjørkum et al., 1998). However, the lack of stylolites and the undeveloped compaction within the study area indicate that the silica responsible for cementation must have come from a different source. Commonly, the alteration of

feldspar causes the release of silica (Thyne et al., 2001). In addition, the associated transformation of montmorillonite and kaolinite to illite may also provide a source of silica (Boles and Franks, 1979; Siebert et al., 1984). As discussed earlier, the homogenization temperature of the fluid inclusions in the quartz doubling in this zone reflects that the formation of siliceous cement, the dissolution of K-feldspar, the montmorillonite illitization, and the conversion of kaolinite to illite take place at the same diagenetic stage. All these different processes may therefore have formed significant contributors for silica within the pore fluid.

5.2.5 Chlorite

The chlorite films are the earliest cement, and may have maintained saline-alkaline conditions within the pore fluid. Chlorite within the studied sandstones are directly related to precipitation from alkaline fluids rich in iron and magnesium. The chlorite films are predominantly developed in sandstones with less matrix in this area, sedimentary microfacies that is related to the strong hydrodynamic conditions that can be found at center bars and point bars (Yang, R. et al., 2014a). The iron and magnesium of the pore lining chlorite are often derived from the rock fragment, biotite, or volcanic ash of mafic to ultramafic composition. Thus the pore lining chlorite often developed at the environment with high iron and magnesium during the sedimentary period (Yang, R. et al., 2014a).

5.2.6 Late calcite cement

The homogenization temperatures of fluid inclusions in calcite cements of the analyzed samples are ranging between 170.33-188.6°C. This indicates that the fluid inclusions were mainly formed during the late diagenetic stage. Late carbonate

cements are commonly related to the supply of CO_2 resulting from the decarboxylation of organic matter in the petroleum system and the availability of Ca^{2+}, Mg^{2+} and Fe^{2+} ions in formation water (Karim et al., 2010). The results of Raman analysis on fluid inclusions in this area show that there are quite a lot of inclusions, which contain CO_2. The same gas was also found in the analysis of the natural gas composition, which demonstrates that there was a release of CO_2 during the evolution of organic matter of the coal deposits the the Sulige area. At the late diagenetic stage, the diagenetic system was nearly closed and the concentration of Ca^{2+} in the pore fluid increased (which was confirmed by fluid inclusion data. In addition, the existing formation water data also confirm the presence of Ca^{2+} in the water), which eventually led to calcite precipitation. Cathodoluminescence shows that the calcite exhibits a bright luminescence, which is related to the lack of iron.

5.3 The early, meso and late diagenetic stages of the Sulige gas field sandstones

5.3.1 Early diagenetic stage

The fluvial-deltaic sedimentary environment and humid paleoclimate were prone to dissolution of debris particles (feldspar, rock fragments and volcanic material). Anorthite can be eroded. Since there is no additional K^+ ion in the water, the calcium feldspar dissolved to form kaolinite, which is accompanied by the release of Ca^{2+}. The reductive rate of the total volume of rock caused by the dissolution of calcium feldspar is only 1.26%. The reaction occurs early, and the formed secondary pores are easily filled by the later cementation, which is difficult to preserve. There are two types of lithic rocks in this area: mafic and felsic. Plagioclase of basic rock debris in blocks with poor circulation of water medium is also easily eroded into kaolinite. Fe^{2+} and Mg^{2+} will be released which is decomposed by pyroxene and amphibole biotite

during minerals dissolution, while acid lithic fragments are difficult to dissolve and they are reserved. The volcanic interstitial matter has different residues because of its different properties. The intermediate base femic constituents are easy to dissolve and a large amount of titanium iron is precipitated, while the intermediate-acid volcanic ash is relatively insoluble, which is dominated by various alteration activities (Yang H. et al., 2007). The release of cations such as Fe^{2+} and Mg^{2+} resulted in an increase of the alkalinity of the water environment, and the decomposition of existing Mg^{2+} and Fe^{2+} in the formation water by medium basic volcanic material, whether it was intermediate basic rock debris or intermediate interstitial material, all of which provide the ion source for the formation of pore lining chlorite. This kind of pore lining chlorite is usually distributed in the place where the clastic grain has ring edge during the deposition period, which is related to the spatial distribution of ferric magnesium deposition material, which promotes the formation of chlorite lining, so, the distribution of iron and magnesium material determines the distribution of chlorite.

In this stage, fluid inclusions are captured only in quartz healing fissures. Fluid inclusions include single-phase brine inclusions and two-phase brine inclusions. The number of two-phase brine inclusions is relatively small, and only five data are obtained (Table 1), combined with initial melting temperature, combined with the initial melting temperature, the H_2O-NaCl-$FeCl_2$ system, H_2O-NaCl-$CaCl_2$ system, and H_2O-$MgCl_2$-$CaCl_2$ system are separated which is corresponding to the initial melting temperature of -36.8°C, -53°C, and -56.6°C, indicating that the fluid is indeed Ca^{2+}, Mg^{2+}, and Fe^{2+} exist, consistent with the above reaction.the initial melting temperature of -42.9°C and -68°C can’t be accurately classified to the system.

Therefore, there is mainly the cementation of kaolinite and chlorite, but it is very few and the pore types are mainly primary intergranular pores and small amounts of dissolved pores at this stage.

In addition, the diagenetic reactions are mainly compaction, calcareous dissolution and kaolinite cementation, and the formation of chlorite cementation, the compaction results in a sharp reduction of pores.

5.3.2 Mesogenetic stage

The thermal simulation experiments in this area show that as the depth of burial depth increases, the organic acid in the coalification process increases gradually and reaches the highest peak (R_o value is approximately 1.59%) before the coal gas peak period, and the coal adsorption capacity is weak at this stage. In the period of time, it was time to expel large amounts of organic acids (Li Z. et al., 2008), it is the most complicated stage of diagenetic reaction at this stage. Organic acids continue to form and enter into adjacent sand layers with compaction and dehydration of clay minerals, resulting in the dissolution of potassium feldspar. The dissolution of potassium feldspar increases the K^+ content in the water, and montmorillonite turns into illite. The maturation of organic matter can accelerate the conversion rate of smectite to illite, which will increase the dissolution rate of potassium feldspar and release more potassium ions (Berger et al., 1997). When montmorillonite is massively converted, which will release $Ca2^+$, Na^+, $Fe2^+$, $Mg2^+$, and OH^- into the water, and causing the acidity of the water to decrease gradually. Above 120°C, the encapsulation of diagenetic system increases with the decrease of water acidity and the increasing of temperature. At this point, the illitization of montmorillonite is roughly stopped, and the diagenetic mineral kaolinite will transform to illite and form an illite precipitate.

Illitization of kaolinite occurs at greater temperatures and high K^+/H^+ activity ratio than dickitization (Lanson et al., 2002), The large number of illite in the area reflects the high K^+/H^+ ratio of diagenetic system, so the quantity of dickite in sandstone is limited. The homogenization temperature of fluid inclusions in quartz doubling is mainly distributed between 79.4 to 148.4°C, which indicates that the silica cementation is mainly formed at this stage, feldspar dissolution, smectite conversion and illitization of kaolinite have the release of Si^{4+}, which promotes the formation of siliceous cements.

In this stage, it will occur the dissolution of feldspar, the formation of siliceous cementation and illite, the pore increment caused by feldspar dissolution in this area is 1.18%, and silica cementation, kaolinite and illite cause pore reductions of 0.72%, 6.36% and 3.25%, respectively. It is important to note that kaolinite and illiteintergranular pores can provide 1.36% and 1.41% additional pore volume, and the porosity decreases to 5.92% at this stage.

The major life-generation and exhaust periods of the Sulige Gas Field are late Jurassic-Early Cretaceous. Compared with the ancient burial history curve, the main exhaust gas temperature range is mainly 120-150 °C. Although methane gas is emitted after 150 °C, it's a limited number. The kaolinite, chlorite, illite and siliceous cementation have already begun to form before the natural gas is fully charged. However, after the filling of natural gas, these kinds of cementates still form, and it is noted that the reservoirs are not formed before they are densified. Rather, it reflects that the characteristics of the Sulige area, which is characterized by the reservoir density and oil-gas accumulation is simultaneously

This diagenetic stage obtained the most fluid inclusion data and the most active water-rock activity, which is consistent with the above study. Combined with the

temperature measurement data of fluid inclusions (Table 1), the developed brine systems are mainly H_2O-$MgCl_2$-$CaCl_2$ type, H_2O-NaCl-$MgCl_2$ type (initial melting temperature is -35°C), H_2O-$CaCl_2$ type (primary melting The temperature is -50 °C), NaCl-$FeCl_2$-H_2O type (initial melting temperature is -37 °C) and H_2O-KCl-$CaCl_2$ (initial melting temperature is -56 °C). It shows that there are many types of ion of the formation fluid and the salinity is also higher.

5.3.3 Late diagenetic stage (temperature:148°C-188°C)

With the increase of burial depth, the evolution of organic matter is dominated by the condensation between the aromatic nuclei. The generated macromolecule hydrocarbons in the early stage are cracked into methane at high temperatures. The diagenetic environment has also changed because of the presence of a large number of metal cations and the lack of supply of organic acids in the middle diagenesis period at the same time. The acidity of the formation water is weakened. Ca^{2+} of the pore fluid reacts with HCO^{3-} to produce calcite. When iron ions are present, it forms iron calcite and blocks the pores. Combined with the temperature measurement data of fluid inclusions, the type of diagenetic fluid developed during this stage is mainly H_2O-$MgCl_2$-$CaCl_2$ (initial melting temperature is -55 °C), and partial inclusions are expressed as H_2O-NaCl-$CaCl_2$ type (primary melting temperature is -53.8 °C), which indicating that**,** the cations of the diagenetic fluid are mainly Na^+, Ca^{2+} and Mg^{2+}etc, while the anions are mainly Cl^-after the diagenetic reaction; the types of ions in the water are reduced, and the salinity also decreases with the precipitation of diagenetic minerals, and water-rock activity weakens. Late calcite makes the reservoir denser.

After the late Cretaceous, it was uplift. Due to the decrease of the temperature and the uplift of the formation, the gas reservoir was in a lost period, and the pressure was gradually reduced, which was forming the present gas reservoir pattern.

The gas reservoir and methane gas were formed at the same time, but the gas reservoir formation was later than a large number of natural gas injections, so that the quality of the reservoir was not greatly affected in the area. It is also explained that although Sulige gas field is a tight gas reservoir, but it was not a tight gas reservoir before the late calcite filling. Therefore, it is favorable for natural gas filling in this area.

5.4 Implications for hydrocarbon exploration and extraction

The physical properties of the sandstone reservoir in the Permian Sulige gas field are characterized by low porosities and permeabilities. In the absence of better reservoirs in this area, exploration and development of tight gas reservoirs, therefore, form the key focus for industry and academia in the Sulige gas field. The sandstone reservoir was densified concomitant with the accumulation of gas. Therefore, the natural gas may incharge into any proper sandstone reservoirs instead of preferential accumulation in high quality reservoir alone. The sandstone may form a possible exploration target if its porosity is not too low, i.e. at least >5% porosity by volume. This may to a large extent increase the exploration range of tight sandstones in the Sulige gas field. The reserve space of the sandstone reservoir is dominanted by intercrystalline pores in kaolinite and illite, which may help to provide necessary information for the exploitation of the tight gas. Especially, these clay minerals have a variety of different effects on the reservoir sensitivity and more detailed knowledge on them (occurrence or absence and distribution within a reservoir) may significantly

help with the design of a development program and the gas reservoir exploitation management.

6. CONCLUSIONS

The sequential order of authigenic mineral formation can be described as follows: chlorite rim - pore lining chlorite - kaolinite - quartz overgrowth+outgrowth - illite - calcite. In the course of secondary mineral precipitation within the sandstones, the diagenetic environment changed from weakly acid (syndiagenetic stage) - weakly alkaline (early Early diagenetic stage) - acid (late Early diagenetic stage to Mesogenetic stage A) - alkaline (Mesogenetic stage B). Although paragenetic sequences such as the afore mentioned sequential order of secondary mineral formation, together with fluid inclusion temperature measurements, can provide significant information on the order of formational processes and their related temperature ranges, for minerals which cannot be measured or have been overlooked during the sampling and analytical process, thermodynamic calculation methods have to be applied in order to speculate on their origin and formation process. Furthermore, the studies for this contribution have shown that the secondary porosity appears to be the main contributor for the reservoir potential of the rocks within the Sulige gas field. The pore types are dominated by intercrystalline pores in illite and kaolinite, matrix solution pores and primary intergranular pore, each of them roughly occupying >10% of the volume of the rock. Corrosion intergranular pores, solution pores in rock fragments, calcite and feldspars, and microcracks take the residual reserve space with <5 Vol.% each.

From the research undertaken for this study, it can be inferred that the tight gas accumulation took place concomitant with densification of the reservoir. The results of this contribution may help to shed new light on the reason and timeframe of the reservoir densification and tight gas accumulation not only in the Sulige gas field, but also in similar tight gas fields world-wide.

ACKNOWLEDGMENTS

This study was supported by the National Natural Science Foundation of China (grant No. 41402120), and Shandong University of Science and Technology Research Fund (grant No. 2015TDJH101).

REFERENCES:

Abouessa, A., Morad, S., 2009. An integrated study of diagenesis and depositionalfacies in tidal sandstones: Hawaz formation (Middle Ordovician), Murzuq Basin, Libya. J. Petrol. Geol. 32, 39-65.

Berger, G., Lacharpagne, J-C., Velde, B., Beaufort, D., Lanson, B., 1997. Kinetic constraints on illitizationreactions and the effects of organic diagenesis in sandstone/shale sequences. Applied Geochem. 12, 23-35.

Bjørkum, P.A., Oelkers, E.H., Nadeau, P.H., Walderhaug, O., Murphy, W.M., 1998. Porosity prediction in quartzose sandstones as a function of time, temperature, depth, stylolite frequency, and hydrocarbon saturation. AAPG Bull. 82, 637-648.

Boles, J.R., Franks, S.G., 1979. Clay diagenesis in Wilcox sandstones of Southwest Texas: implications of smectite diagenesis on sandstone cementation. J. Sediment. Petrol. 49, 55-70.

Brantley. S., Stillings L., 1996. Felspar dissolution at 25℃ and low pH. Amer. J. Sci. 296, 101-127.

Brosse, É., Margueron T., Cassou C., Sanjuan, B., Canham, A., Girard, J.-P., Lacharpagne, J.-C., Sommer, F., 2003. The formation and stability of kaolinite in Brent sandstone reservoirs: A modeling approach. In: Worden, R.H., Morad S. (eds.) Clay mineral cements in sandstones. Inter. Assoc. Sedimentol. Spec. Pub. 34, 383-408.

Cao, M., Yao, J., Deng, X., Yang, F., Mao G., Mathur, R., 2017. Diverse and multistage Mo, Au, Ag–Pb–Zn and Cu deposits in the Xiong'er Terrane, East Qinling: From Triassic Cu mineralization. Ore. Geol. Rev. 81, 565-574.

Carroll, A.R., Grahamwand, S.A., Smith, M.E., 2010. Walled sedimentary basin of China. Basin Res. 22, 17–22.

Darby, B.J., Ritts, B.D., 2002. Mesozoic contractional deformation in the middle of the Asian tectonic collage, the intraplate western Ordos Fold∼Thrust Belt China. Earth Planet. Sci Lett. 205, 13–24.

Dong, Y., Zhang, G., Neubauer, F., Liu, X., Genser J., Hauzenberger C., 2011. Tectonic evolution of the Qinling Orogen, China: Review and synthesis. J. Asian Earth Sci. 41, 213-237.

Dong, Y., Zhang, X., Liu, X., Liu, X., Li,W., Chen, Q., Zhang,G., Zhang,H., Yang,Z., Sun, S., Zhang, F., 2015. Propagation tectonics and multiple accretionary processes of the Qinling Orogen. J. Asian Earth Sci. 104 S1, 84-98.

Du, Q., Han, Z., Shen, X., Gao,L., Han, M., Song, Z., Li, J., Zhong, W., Yan J., Liu H., 2017. Geochemistry and geochronology of Upper Permian–Upper Triassic volcanic rocks in eastern Jilin Province, NE China: implications for the tectonic evolution of the Palaeo-Asian Ocean. Intern. Geol. Rev. 59, 368-390.

Du, Q., Han, Z., Shen, X., Han, C., Song, Z., Gao, L., Han, M., Zhong, W., Yan, J., 2017. New Evidence of Detrital Zircon Ages for the Final Closure Time of the Paleo-Asian Ocean in the Eastern Central Asian Orogenic Belt (NE China). Acta Geol. Sinica 91, 1910-1914.

Dutton,S.P., Diggs,T.N., 1990. History of quartz cementation in the Lower Cretaceous Travis peak formation, East Texas. J. Sed. Petrol. 60,191-202.

Egeberg, P., Aagaard, P., 1989. Origin and evolution of formation waters from oil fields on the Norwegian shelf. Applied Geochem. 4, 131-142.

Ehrenberg, S., 1989. Assessing the importance of compaction processes and cementation to reduction of porosity in sandstones: discussion; compaction and porosity evolution of Pliocene sandstones, Ventura Basin, California: discussion. APPG Bull. 73, 1274-1276.

Ehrenberg, S., Jakobsen, K., 2001. Plagioclase dissolution related to biodegradation of oil in brent group sandstones (Middle Jurassic) of Gulffaks field, northern North Sea. Sedimentology 48, 703-721.

Ehrenberg, S.N., 1993. Preservation of anomalously high porosity in deeply buriedsandstones by grain-coating chlorite: examples from the Norwegiancontinental shelf. Amer. Assoc. Petrol. Geol. Bull. 77, 1260–1286.

Hammer, E., MØrk, M.B., Naess A., 2010. Facies controls on the distributin of diagenesis and compaction in fluvial-deltaic deposits. Mar. Petrol. Geol. 27, 1737-1751.

Fan, A., Yang, R., Feng, Q., Liu, Y., Han, Z., 2006. Application of fluid inclusion to study of natural gas geology in Ordos basin. J. China Univ. Min. Tech. 16,439-442.

Fan, A., Yang, R., Li. J., Zhao, Z., Van Loon, A. J., 2017. Siliceous cementation of chlorite- coated grains in the Permian sandstone gas reservoirs, Ordos Basin. Acta Geologica Sinica 91, 11473-1148.

Fan, A., Yang, R., Van Loon, A.J., Yin,W., Han, Z., Zavala, C., 2018. Classification of gravity-flow deposits and their significance for unconventional petroleum exploration, with a case study from the Triassic Yanchang Formation (southern Ordos Basin, China). J. Asian Earth Sci. 161, 57-73.

Folk, R.L., 1980. The Petrology of Sedimentary Rocks. Hemphill Publishing Company, Austin, TX, 127.

Harris, N.B., 1992. Burial diagenesis of Brent sandstones: a study of Statfjord, Hutton and Lyell fields. In: Morton, A.C., Haszeldine, R.S., Giles, M.R., Brown, S. (Eds.), Geology of the Brent Group. Geol. Soc. Lond. Spec. Pub. 61, 351-375.

Huang, S., Huang, K., Feng, W., Tong, H., Liu, L., Zhang, X., 2009. Mass exchanges among feldspar, kaolinite and illite and their influences on secondary porosity formation in clastic diagenesis — A case study on the Upper Paleozoic, Ordos Basin and Xujiahe Formation, Western Sichuan Depression. Geochimica 38, 498-506.

Karim, A., Pe-Piper, G., Piper, David J.W., 2010. Controls on diagenesis of Lower Cretaceous reservoir sandstones in the western Sable Subbasin, offshore Nova Scotia. Sediment. Geol. 224, 65-83.

Khalifa, M., Morad, S., 2008. Impact of depositional facies on the distribution of diagenetic alterations in the Devonian shoreface sandstone reservoirs,Southern Ghadamis Basin,Libya. Sediment. Geol. 329, 62-80.

Khalifa, M., Morad, S. , 2012. Impact of structural setting on diagenesis of fluvial and tidal sandstones: The Bahi Formation, Upper Cretaceous, NW Sirt Basin, North Central Libya.Marine and Petroleum Geology 38, 211-231.

Lanson, B., Beaufort, D., Berger, G., Bauer, A., Cassagnabere, A., Meunier, A., 2002. Authigenic kaolin and illitic minerals during burial diagenesis of sandstones: a review. Clay Minerals 37, 1-22.

Lewis, D.W., 1989. Applied sedimentology. Geological press, 5-33.

Li, X.P., Yang, Z., Zhao, G., Grapes, R., Guo, J., 2011. Geochronology of khondalite-series rocks of the Jining Complex: confirmation of depositional age and tectonometamorphic evolution of the North China Craton. Intern. Geol. Rev. 53, 1194–1211.

Li, X.P., Yan, J.Y., Schertl, H.P., Kong, F.M., Xu, H., 2014. Eclogite from the Qianliyan Island in the Yellow Sea: a missing link between the mainland of China and the Korean peninsula. Eur. J. Mineral. 26, 727–741.

Li, X.P., Chen, H.K., Wang, Z.L., Wang, L.J., Yang, J.S., Robinson, P., 2015. Textural evolution of spinelidotite and olivine websterite in the Purang Ophiolite Complex, western Tibet. J. Asian Earth Sci. 10, 55–71.

Li, X.P., Duan, W.Y., Zhao, L.Q., Schertl, H.P., Kong, F.M., Shi, T.Q., Zhang, X., 2017. Rodingites from the Xigaze ophiolite, southern Tibet—new insights into the processes of rodingitization. Eur. J. Miner. 29. 821-837.

Li, Z., Hui, K., Li, L., 2008. Analysis of Characteristics of Gas Migration and Reservoir-Forming in the Upper Paleozoic of Northern Ordos Basin. J. Miner. Petrol. 28, 77-83 in Chinese with English abstract.

Liu, L., Kang, L., Cao, Y., Yang, W., 2015. Early Paleozoic granitic magmatism related to the processes from subduction to collision in South Altyn, NW China. Sci. China (Earth Sci.) 58, 1513−1522.

Mao, G., Liu, C., Zhang, D., Qiu,X., Wang, J., Liu, B., Liu, J., Deng, Y., Wang, F., Zhang, C., 2014. Effects of uranium on hydrocarbon generation of hydrocarbon source rocks with type-III kerogen. Sci. China Earth Sci. 57, 1168-1179.

McBride,E.F.,1989. Quartz cement in sandstones -:a review. Earth Sci. Rev. 26, 69-112.

Meng, W., Lu, Z., Feng, M., Zhang, S., Li, M., Mai, F, 2011. The origin of tight sandstone authigenic Illite and its influence on the development of relatively high quality reservoirs: taking the reservoir of the fourth member of Xuzhou formation in western Sichuan as an example. Acta Petrol. Sinica 32, 783-790 in Chinese with English abstract.

Milliken, K.R., McBride, E.F., Land, L.S., 1989. Numerical assessment of dissolution versus replacement in the subsurface destruction of detrital feldspars, Oligocene Frio Formation, South Texas. J. Sediment. Petrol. 59, 740-757.

Min, Q.,Yang, H., Fu J., 2000. Deep Basin Gas in Ordos Basin. Nat. Gas Ind. 20, 11-15 in Chinese with English abstract.

Morad, S., 1998. Carbonate cementation in sandstones: distribution patterns and geochemical evolution. In: Morad, S. (Ed.), Carbonate Cementation in Sandstones. Intern. Assoc. Sediment., Spec. Pub. 26, Blackwell, Oxford.1-26.

Morad, S., Al-Aasm, I., Ramseyer, K., Marfil, R., Aldahan, A., 1990. Diagenesis of carbonate cements in permo-triassic sandstones from the Iberian Range, Spain: evidence from chemical composition and stable isotopes. Sediment. Geol. 67, 281-295.

Morad, S., De Ros, L.F., 1994. Geochemistry and diagenesis of strata bound calcitecement layers within the rannoch Formation of the Brent Group, MurchisonField, North Viking Graben (northern North Sea), discussion and reply. Sediment. Geol. 93, 135–147.

Morad, S., Ketzer, J., De Res, L., 2000. Spatial and temporal distribution of diagenetic alterations in siliciclastic rocks: implications for mass transfer in sedimentary basins. Sedimentology 47, 95-120.

Qiu, X., Liu, C., Mao, G., Deng, Y., Wang, F., 2014. Late Triassic tuff intervals in the Ordos basin, central China: their depositional, petrographic, geochemical characteristics and regional implications. J. Asian Earth Sci. 80, 148–160.

Sanjuan, B., Girard, J., Lanini, S., et al. 2003. Geochemical Modelling of Diagenetic Illite and Quartz Cement Formation in Brent Sandstone Reservoirs: Example of the Hild Field, Norwegian North Sea. Clay Mineral Cements in Sandstones. Blackwell Publishing Ltd., 425-452.

Shaw, H., Conybeare, D., 2003. Patterns of clay mineral diagenesis in interbedded mudrocks and sandstones: an example from the Palaeocene of the North Sea. Spec. Pub. Intern. Assoc. Sediment. 34, 129-145.

Siebert, R.M., Moncure, G.K., Lanhann, R.W., 1984. A theory of framework grain dissolution in sandstones. In: McDonald, D.A., Surdam, R.C. (Eds.), Clastic Diagenesis. AAPG Mem. 37, 163-176.

Song, Z., Li, J., Gu, Z., Tang, W., Yu, J., Gao, L., 2016. Characteristics of buried paleochannels in the western South Yellow Sea during the last glaciations. Tech. Gazette 23, 835–842.

Stonecipher., S., Winn Jr. R. Bishop., M., 1984. Diagenesis of the frontier formation,Moxa Arch:a function of sandstone geomentry,texture and composition,and fluid flux. AAPG Bull. 68, 289-316.

Storvoll, V., Bjørlykke, K., Karlsen, D., Saigal, G., 2002. Porosity preservation in reservoir sandstones due to grain-coating illite: a study of the Jurassic Garn Formation from the Kristin and Lavrans fields, offshore Mid-Norway. Mar. Petrol. Geol. 19, 767-781.

Surdam, R., Boese, S., Crossey, L., 1984. The chemistry of secondary porosity. AAPG Bull. 37, 127-149.

Thyne,G., Boudreau,B.P., Ramm,M., Midtbo,R.E., 2001. Simulation of potassium feldspar dissolution and illitization in the Statfjord Formation,North Sea. APPG Bull. 85, 621-635.

Stroker, T.M., Harris, N.B., Elliott, W.C., Wampler, J.M., 2013. Diafenesis of a tight gas sand reservoir:Upper Cretaceous Mesaverde Group, Piceance Basin, Colorada. Mar. Petrol. Geol. 40, 48-68.

Wang C., Gao L., Xu H.,Yin W., Chen X., Liu C., Li S., 2011. The mechanism of deep basin gas formation and the division of reservoir forming stage-taking Ordos Basin as an example. Natural Gas Geosci. 22, 15-22 in Chinese with English abstract.

Wang, G., Chang, X., Yin, W., Li, Y., Song, T., 2017. Impact of diagenesis on reservoir quality and heterogeneity of the Upper Triassic Chang 8 tight oil

sandstones in the Zhenjing area Ordos Basin, China. Mar. Petrol. Geol. 83, 84–96.

Wang, Q., Hao, L., Chen, G., Zhang, G., Zhang, R., Ma, X., Wang, H., 2010. Formation mechanism of carbonate cementation in the sandstone of Zhuhai formation in Baiyun sag. Acta Petrol. Sinica 31, 553-559 in Chinese with English abstract.

Weber, J., Ricken, W., 2005. Quartz cementation and related sedimentary architecture of the Triassic Solling Formation, Reinhardswald Basin, Germany. Sediment. Geol. 175,459-477.

Wei, W., Huang, S., Huan, J., 2011. Thermodynamic calculation of the reaction of Illite formation and its significance to the study of sandstone diagenesis. Geol. Sci. Tech. Inform. 30: 20-25.

Wilkinson, M., Milliken, K.L., Haszeldine, R.S., 2001. Systematic destruction of K-feldspar in deeply buried rift and passive margin sandstones. J. Geol. Soc. Lond. 158, 675-683.

Wilkinson, M., Haszeldine, R., Milliken, K., 2003. Cross-Formational flux of aluminium and potassium in Gulf Coast(USA) sediments. Spec. Pub. Intern. Assoc. Sediment. 34, 147-160.

Wilson, M.D., Stanton, P.T., 1994. Diagenetic mechanisms of porosity and permeability reduction and enhancement. In: Wilson MD (ed). Reservoir Quality Assessment and Prediction in Clastic Rocks. SEPM Short Course 30,59-118.

Worden, R. H., Morad, S., 2003a. Clay minerals in sandstones: controls on formation,distribution and evolution. In: Worden, R.H., Morad, S. (Eds.), Clay MineralCements in Sandstones. Intern. Assoc. Sediment. Spec. Pub. 34, Blackwell, Oxford, 3-41.

Worden, R., H., Morad, S., 2003b. The Formation and Stability of Kaolinite in Brent Sandstone Reservoirs: A modelling Approach// Clay Mineral Cements in Sandstones. Intern. Assoc. Sediment. Spec. Pub. 34, Oxford: Blackwell Pub. Ltd., 383-408.

Worden, R., Oxtoby, N., Smalley, P., 1998. Can oil emplacement prevent quartz cementation in sandstones? Petrol. Geosci. 4, 129-137.

Worden, R.H., Morad, S., 2009. Quartz cementation in oil field sandstones: a review of the key controversies. In Worden, R.H., Morad, S. (Eds.), Quartz Cementation in Sandstones. Blackwell Pub. Ltd., Oxford, UK., 11-27.

Xie, X., Heller, P.L., 2013. U-Pb detrital zircon geochronology and its implications: The early Late Triassic Yanchang Formation, south Ordos Basin, China. J. Asian Earth Sci. 64, 86–98.

Yang, H., Yang, Y., Shi, X., Yin, P., 2007. Influence of the late Paleozoic volcanic activity on the sandstone reservoir in the interior of Ordos Basin. Acta Sedment. Sinica 25, 526-534 in Chinese with English abstract.

Yang, H., Fu, J., Liu, X., Fan, L., 2012. Formation conditions and exploration techniques of Sulige large tight sandstone gas reservoir. Acta Petrolei Sinica 33 (1), 27-36.

Yang, H., Liu, X., 2014. Progress in coal gas exploration of Paleozoic in Ordos Basin. Petrol. Explor. Dev. 44, 129-137.

Yang, R., Fan, A., Van Loon, A. J., Han, Z., Wang, X., 2014a. Depositional and diagenetic controls on sandstone reservoirs with low porosity and low permeability in the eastern Sulige gas field, China. Acta Geologica Sinica 88, 1513-1534.

Yang, R., He, Z., Qiu, G., Jin, Z., Sun, D., Jin, X., 2014b. A Late Triassic gravity flow depositional system in the southern Ordos Basin. Petrol. Explor. Dev. 41, 724-733.

Yang, R., Jin, Z., Van Loon, A.J., Han, Z., Fan, A., 2017. Climatic and tectonic controls of lacustrine hyperpycnite origination in the Late Triassic Ordos Basin, central China: implications for unconventional petroleum development. AAPG Bull. 101, 95-117.

Yang, R., Fan, A., Han, Z., Van Loon, A.J., 2017b. Lithofacies and origin of the Late Triassic muddy gravity-flow deposits in the Ordos Basin, central China. Mar. Pet. Geol. 85, 194–219.

Yang, R., Van Loon, A.J., Fan, A., Han, Z., Jin,X., Jin,Z., Han, Z., Fan, A., Liu, Q., in press. From divergent to convergent plates: Resulting facies shifts along the southern and western margins of the Sino-Korean Plate during the Ordovician. J. Geodyn. doi.org/10.1016/j.jog.2018.02.001.

Yang Y., Bao H., Jia Y.,Yu Z., 2008. Analysis of controlling factors of Upper Paleozoic sandstone reservoir in Ordos Basin. J. Palaeogeo. 10 (1), 25-32.

Zhang, J., Zhang, P., Xie, J., 2013. Diagenesis of Clastic Reservoirs: Advances and Prospects, Advances in Earth Sci. 28, 957-967 in Chinese with English abstract.

Zhang, W., Guo, Y., Tang, D., 2009. Characteristics of fluid inclusions in Upper Paleozoic reservoirs and their hydrocarbon accumulation stages in Sulige Gas Field. Acta Petrolei. Sinica 30 (5), 685-691 in Chinese with English abstract.

Zheng, J., Ying, F., 1997. Reservoir Characteristics and Diagenetic Model of Sandstone intercalated in Coal-Bearing Strata (Acid water medium). Acta Petrolei. Sinica 18, 19-24.

Zhu, R., Zou, C., Zhang, N., Wang, X., Cheng, R., Liu, L., Zhou. C., Song, L., 2009. Diagenetic fluid Evolution and Genesis Mechanism of tight Sandstone Gas reservoirs: a case study of Xujiahe Formation of Upper Triassic in Sichuan Basin. Sci. China (Earth Sci.) 39, 327-339.

Figure-1. Tectonic setting, structural division of the Ordos Basin, location of the study area and Sulige Gas field, and sedimentary facies of the Middle Permian. The insert map shows the location of the Ordos Basin in China.

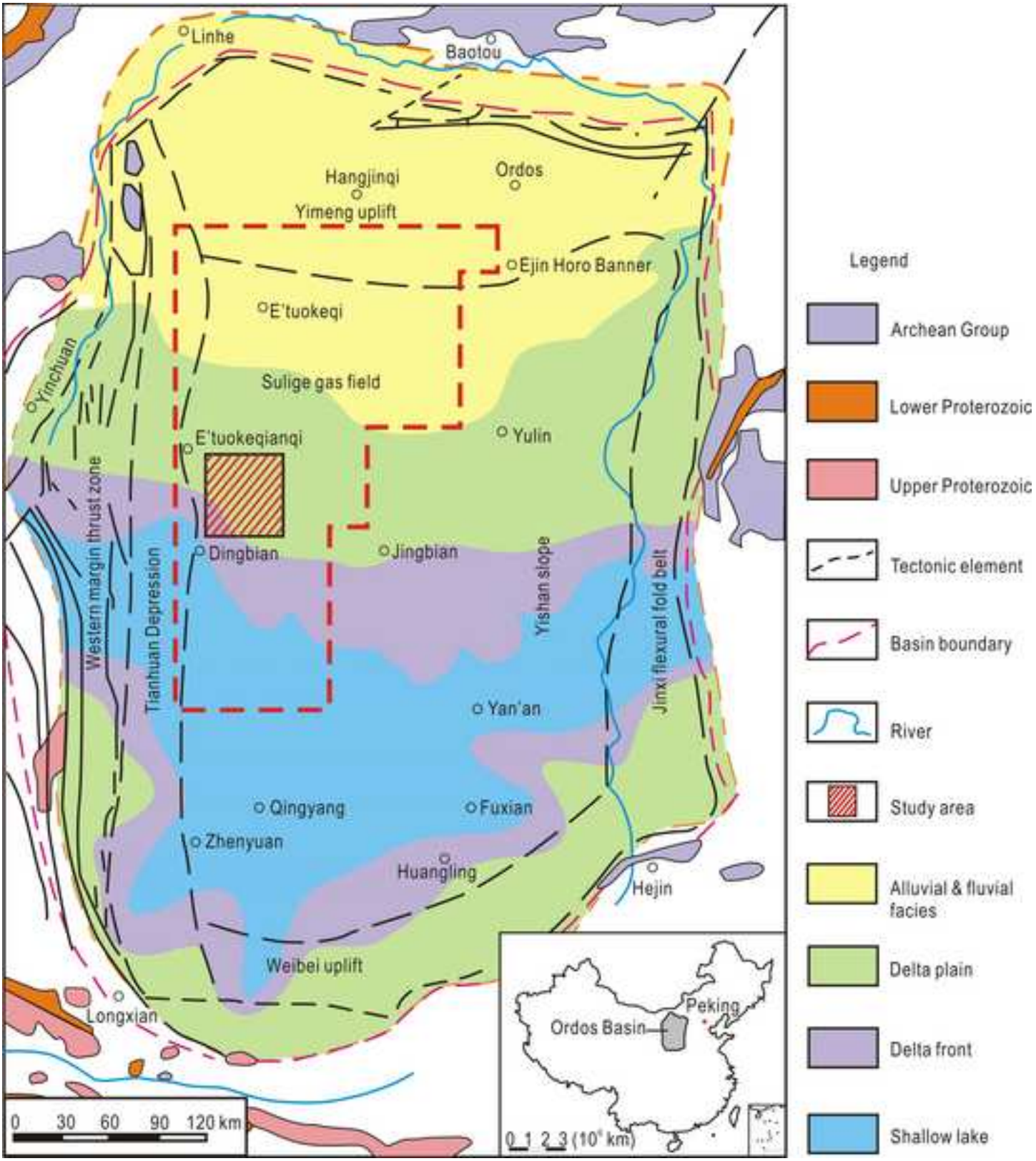

Figure-2. A. Strata of the Upper Paleozoic, simplified lithology, marker bed, and gas members of the Permian System. B. Representative logging curves, lithology and detailed sedimentary facies in the main gas productive layer, the upper section of the lower Permian Shanxi Formation (P1s1) and the 8th member of the middle Permian Shihezi Formation (P_2h_8).

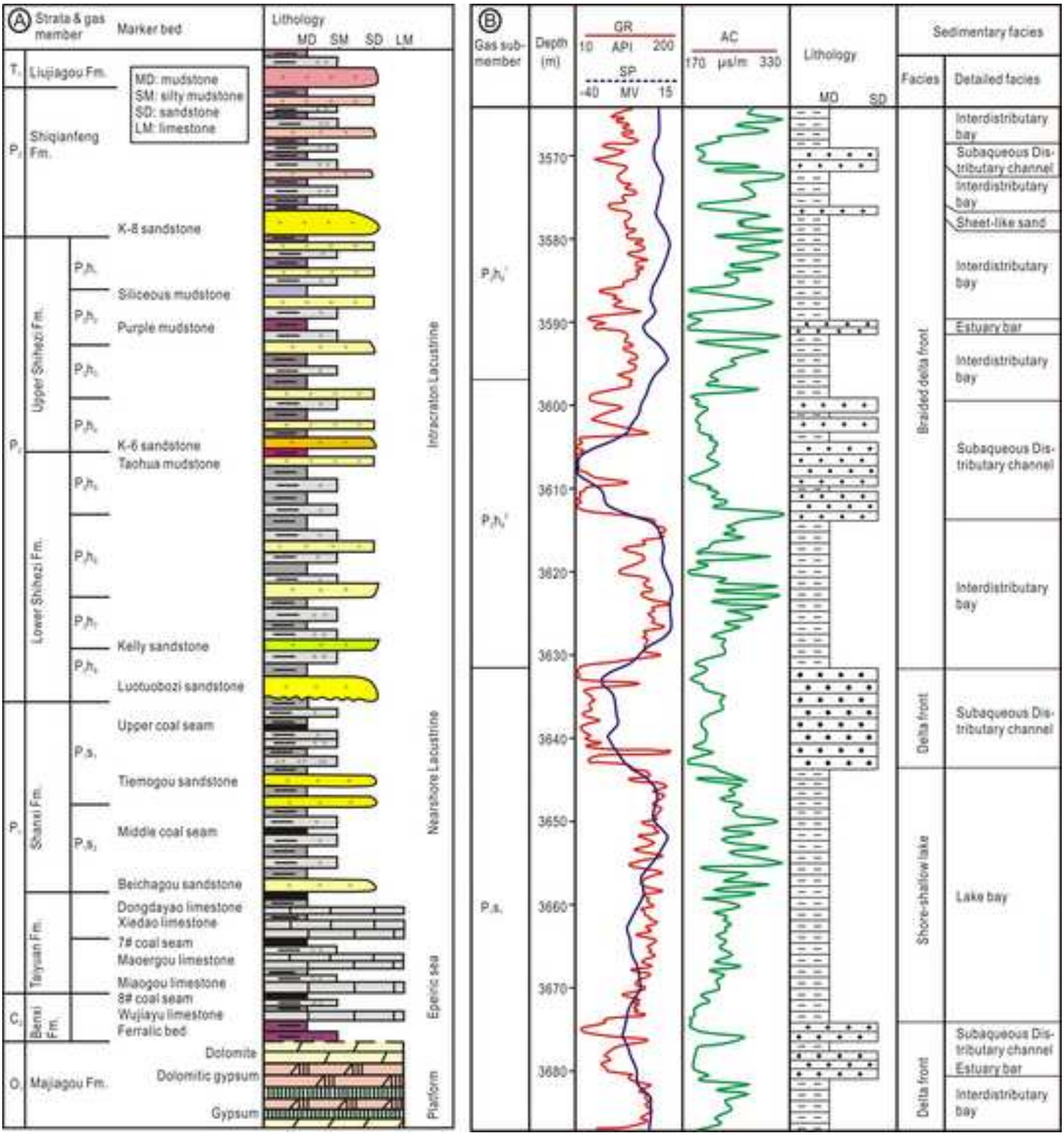

Figure-3. A N-S extending geological model of the Upper Paleozoic tight gas reservoir in the Ordos Basin, showing its source rocks, reservoirs and caprocks (after Yang and Liu, 2014). P_2h_u, the upper Shihezi Formation; P_2h_l, the lower Shihezi Formation; P_1s, Shanxi Formation; P_1t, Taiyuan Formation; C_2b, Benxi Formation.

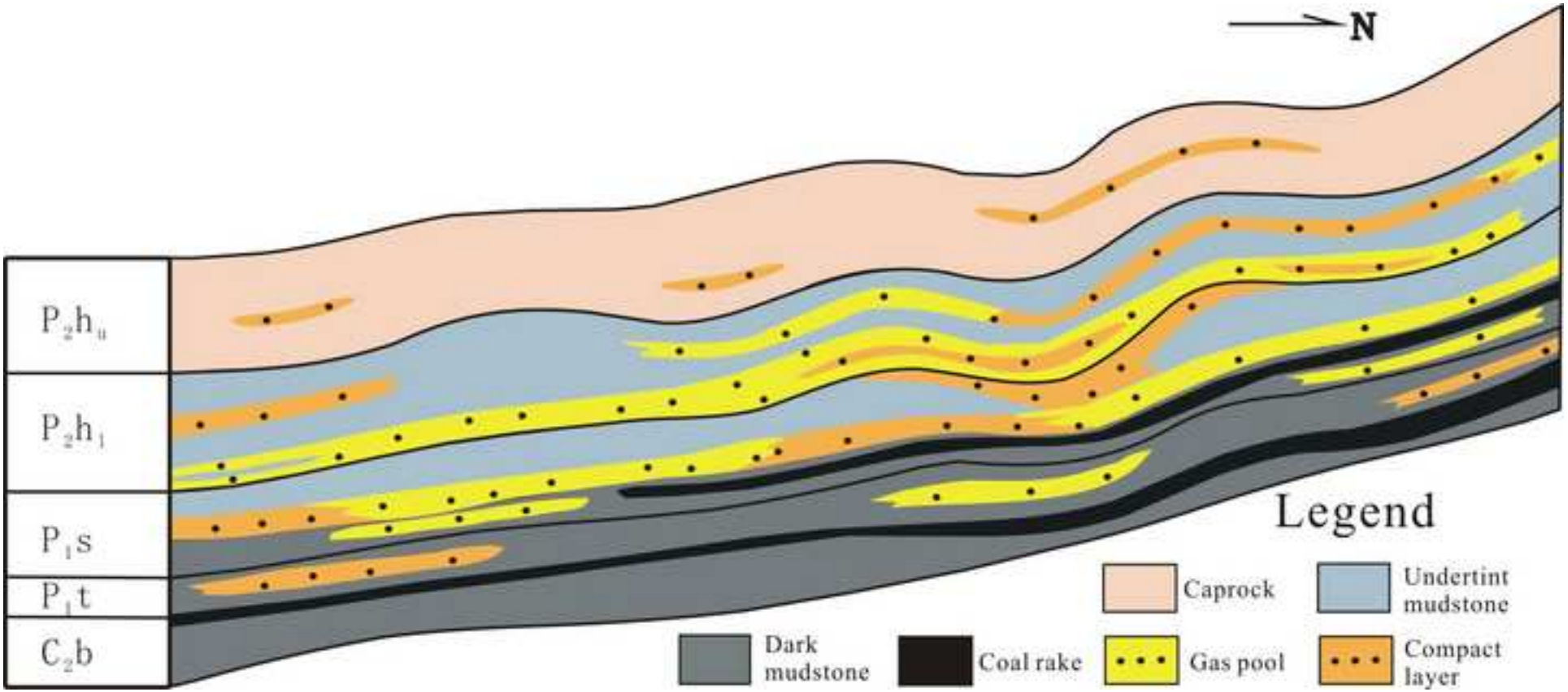

Figure-4. Burial history curves, tectonic evolution, geothermal isogram and reflectance of vitrinite isolines in the study area, Sulige gas field (modified from Zhang et al., 2009).

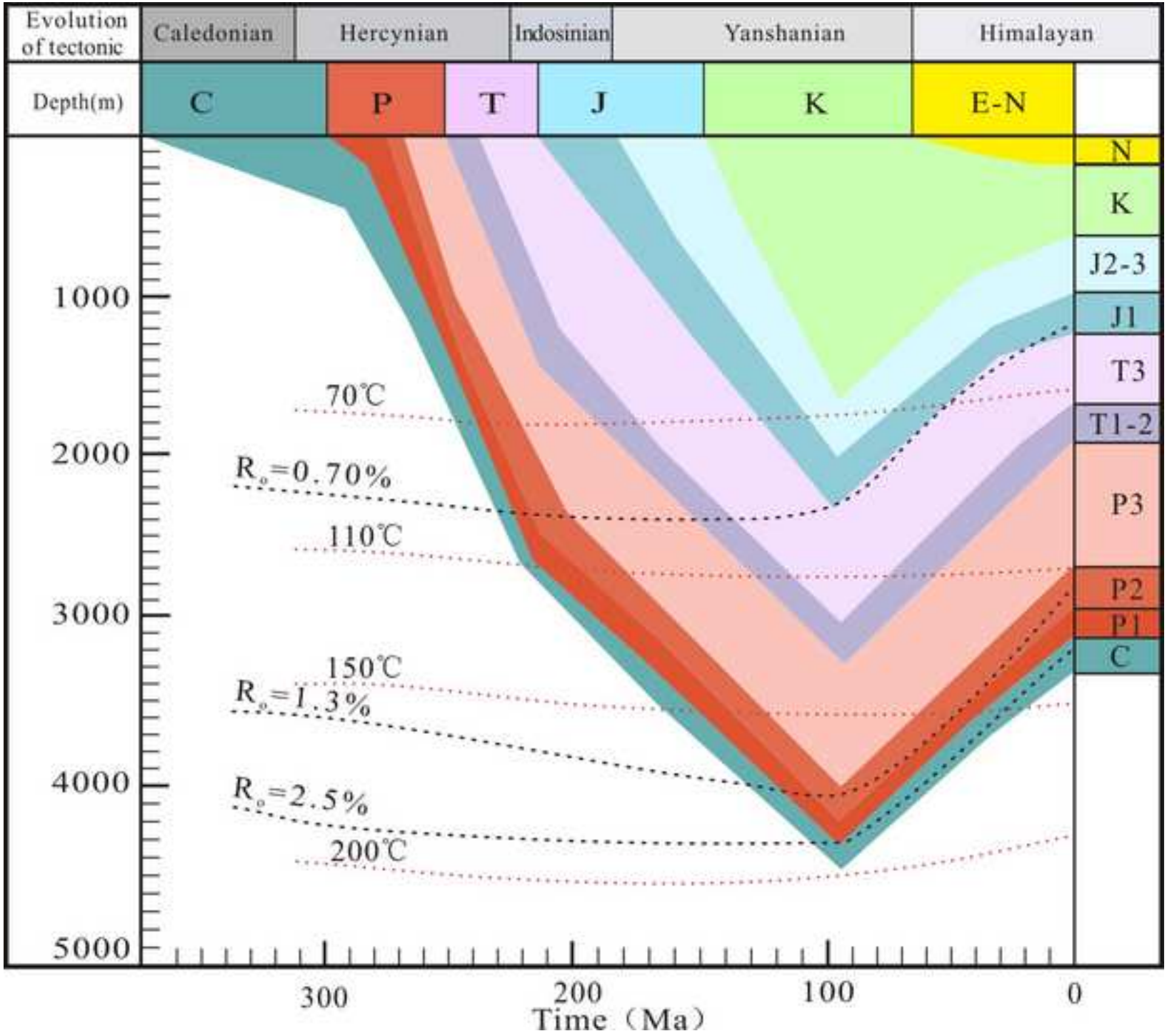

Figure-5. Cores of the main gas reservoir in the P_1s_1 and P_2h_8, Sulige gas field. A. massive grayish gravelly sandstone, well T25, 2827.99 m, P_2h_8; B. massive grayish coarse sandstone, well T26, 2836.28 m, P_2h_8; C. unclear small-scale cross bedding, grayish medium sandstone, well T26, 2837.01 m, P_2h_8; D. unclear parallel bedding, greenish-gray fine sandstone, well Z21, 3077.67 m, P_2h_8; E. massive greenish-gray gravelly sandstone, well T26, 2853.46 m, P_1s_1; F. massive gray coarse sandstone, well T26, 2852.47 m, P_1s_1; G. unclear parallel bedding, greenish-gray medium sandstone, well Z21, 3091.23 m, P_1s_1; H. small-scale ripples, greenish-gray medium sandstone, well Z24, 2946.42 m, P_1s_1.

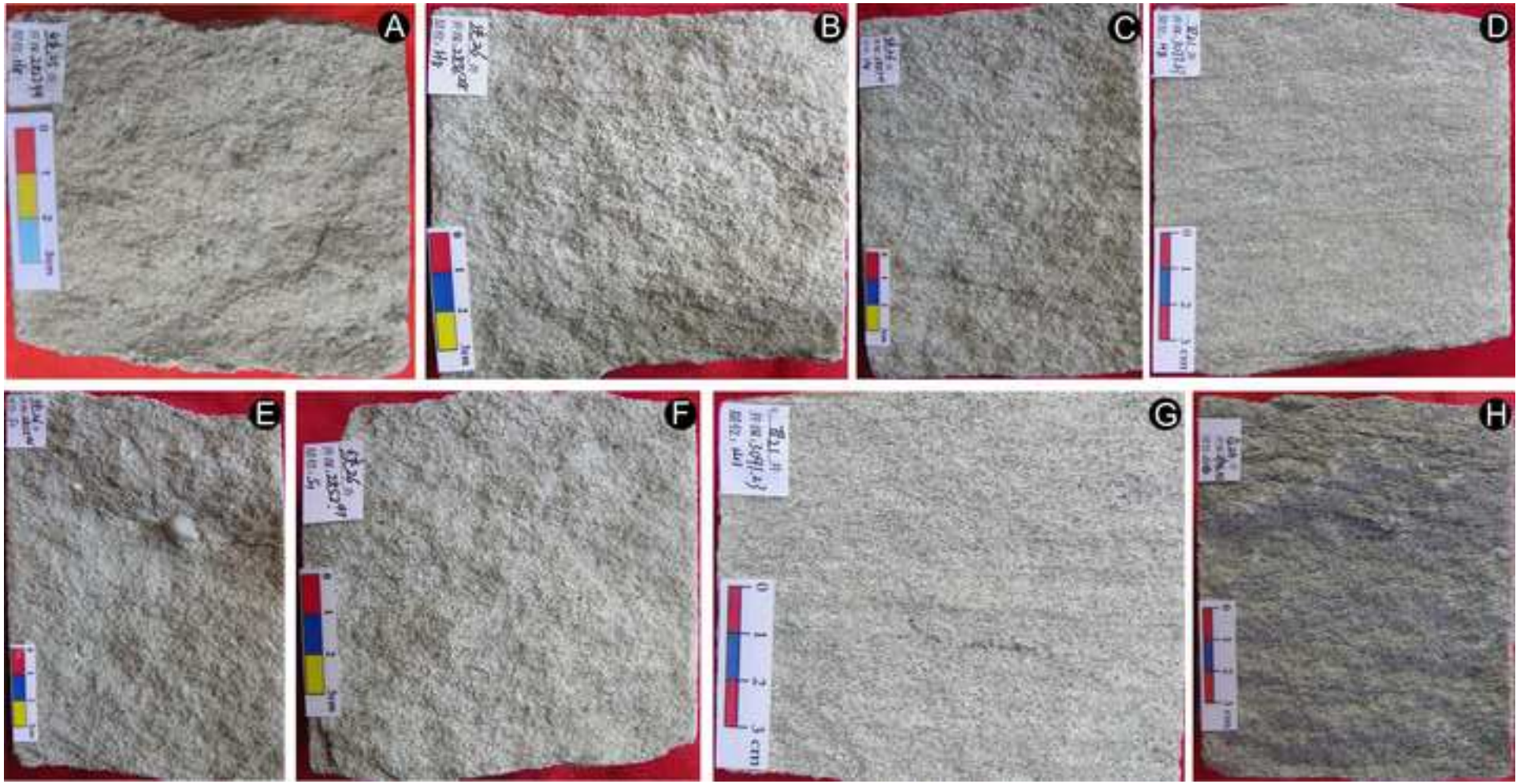

Figure-6. Lithologic triangular plot of the main gas reservoir in the P_1s_1 and P_2h_8, Sulige Gas field (modified from Folk, 1968).

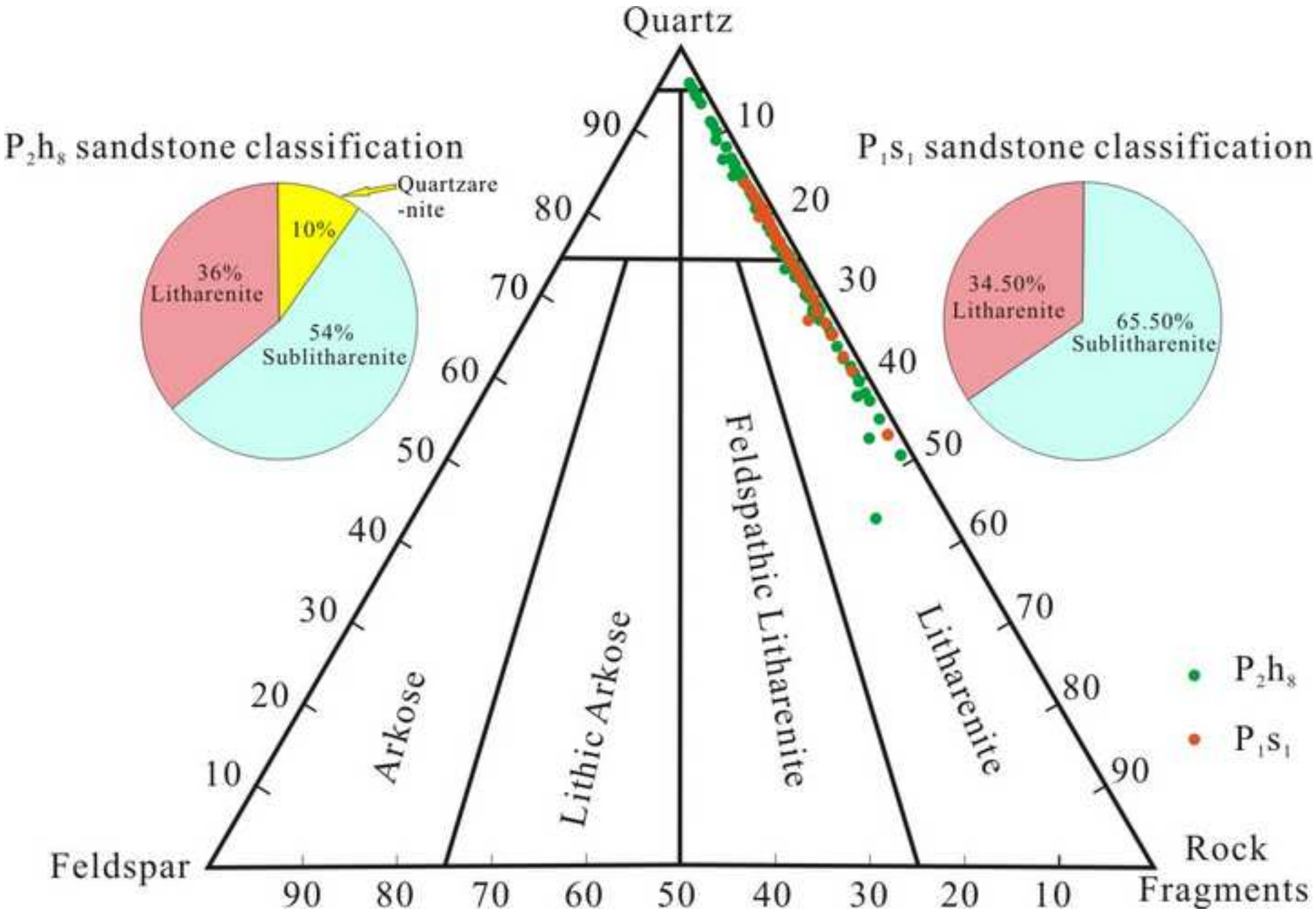

Figure-7. Dissolution pores (red resin) of feldspar, rock debris and occurrences of kaolinite. A. dissolution pores of feldspar and intercrystalline pores of kaolinite, well T32, 2684.44 m, P_2h_8; B. dissolution pores of rock fragment, well T29, 2782.88 m, P_2h_8; C. dissolution pores of plagioclase and kaolinite, well T32, 2736.5 m, P_2h_8; D. dissolution pores of plagioclase and intercrystalline pores of kaolinite, well Z24, 2922.28 m, P_2h_8; E. dissolution pores of rock debris, residual intergranular pores and pore-filling kaolinite, well Z14, 3027.19 m, P_2h_8; F. dissolution pores of rock debris and precipitation of kaolinite, well Z9, 3042.51 m, P_1s_1.

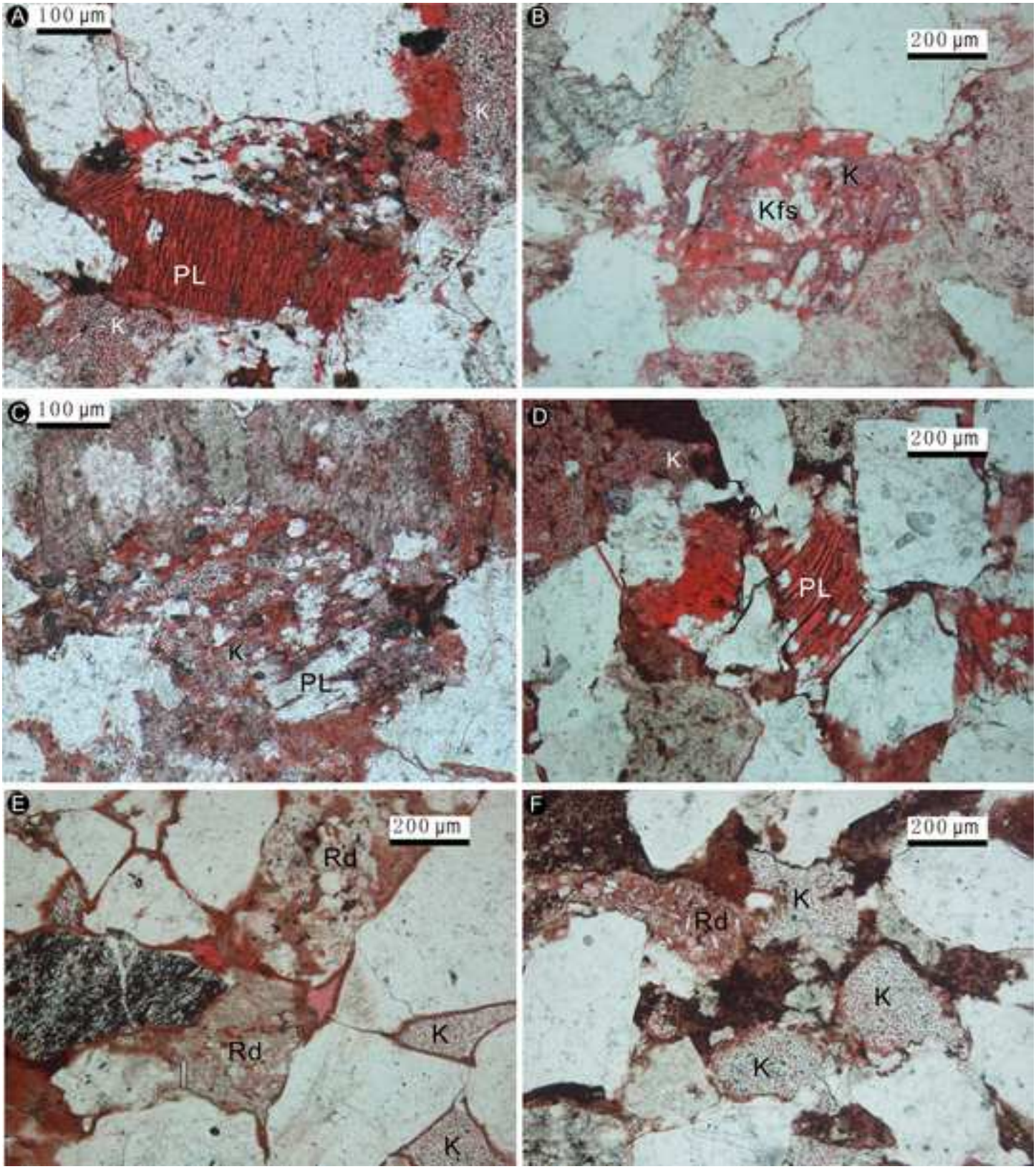

Figure-8. X-ray diffraction of clay minerals in the sandstone reservoir, Sulige gas field. Well Z12, 3122.75 m.

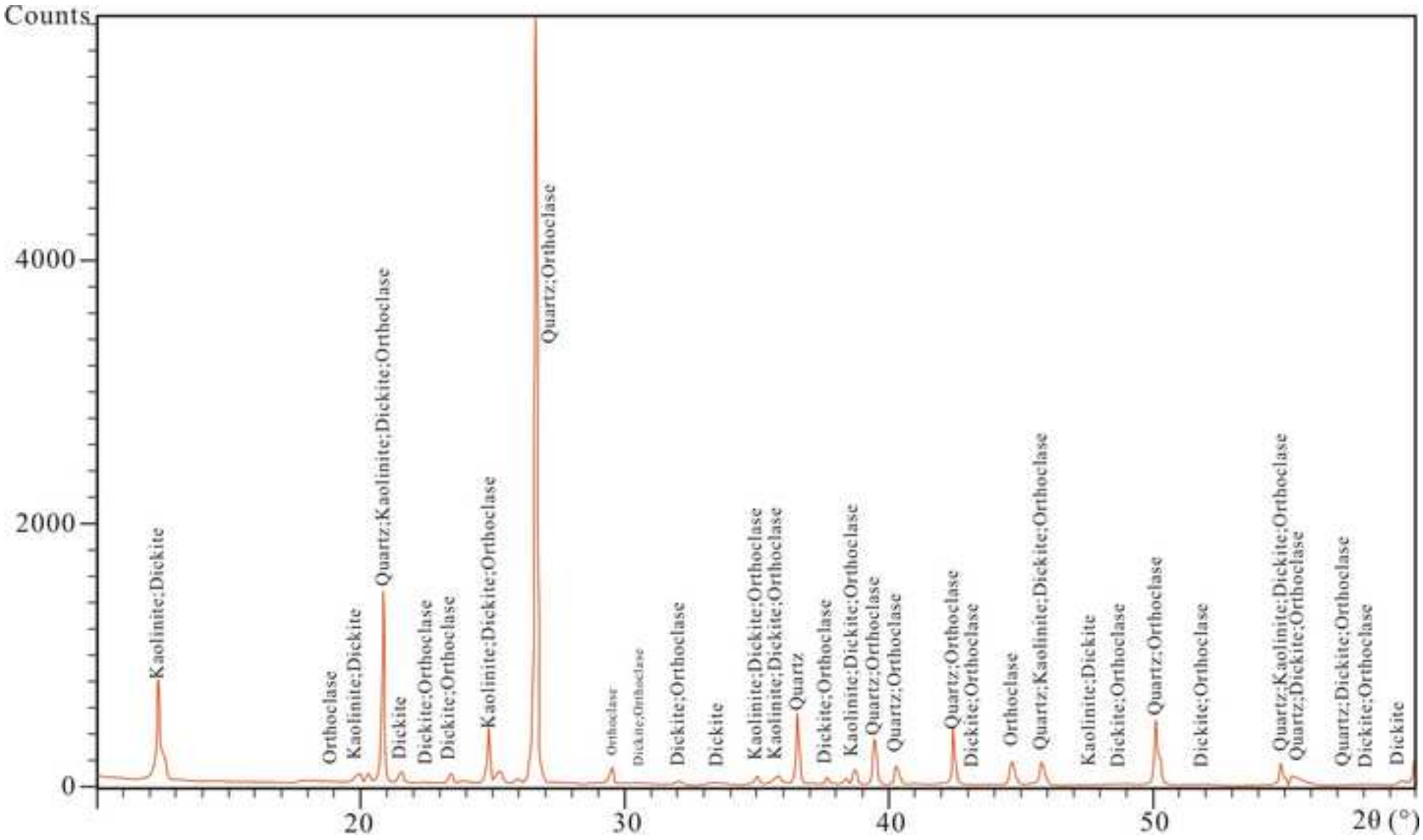

Figure-9. Microfeatures of illite, kaolinite, dickite, smectite illitization, K-feldspar dissoluted into illite, quartz grains and pores in the P_1s_1 and P_2h_8, Sulige Gas field. A. co-existence of illite, kaolinite and dickite, and intercrystalline pores, well Tong25, 2802.19 m, SEM, P_2h_8; B. quartz overgrowth, illite and residual intergranular pores, well S315, 3672.20 m, P_2h_8, plane polarized light; C. quartz overgrowth, illite and residual intergranular pores, well S315, 3672.20 m, P_2h_8, cross polarized light; D. curved and broken feldspar, illite and kaolinite, well Z30, 3072.20 m, P_1s_1, cross polarized light; E. Dissolution of feldspar and formation of illite, well Tong25, 2816.68 m, P_1s_1, SEM; F. illitization of smectite, well Tong25, 2802.19 m, P_2h_8, SEM.

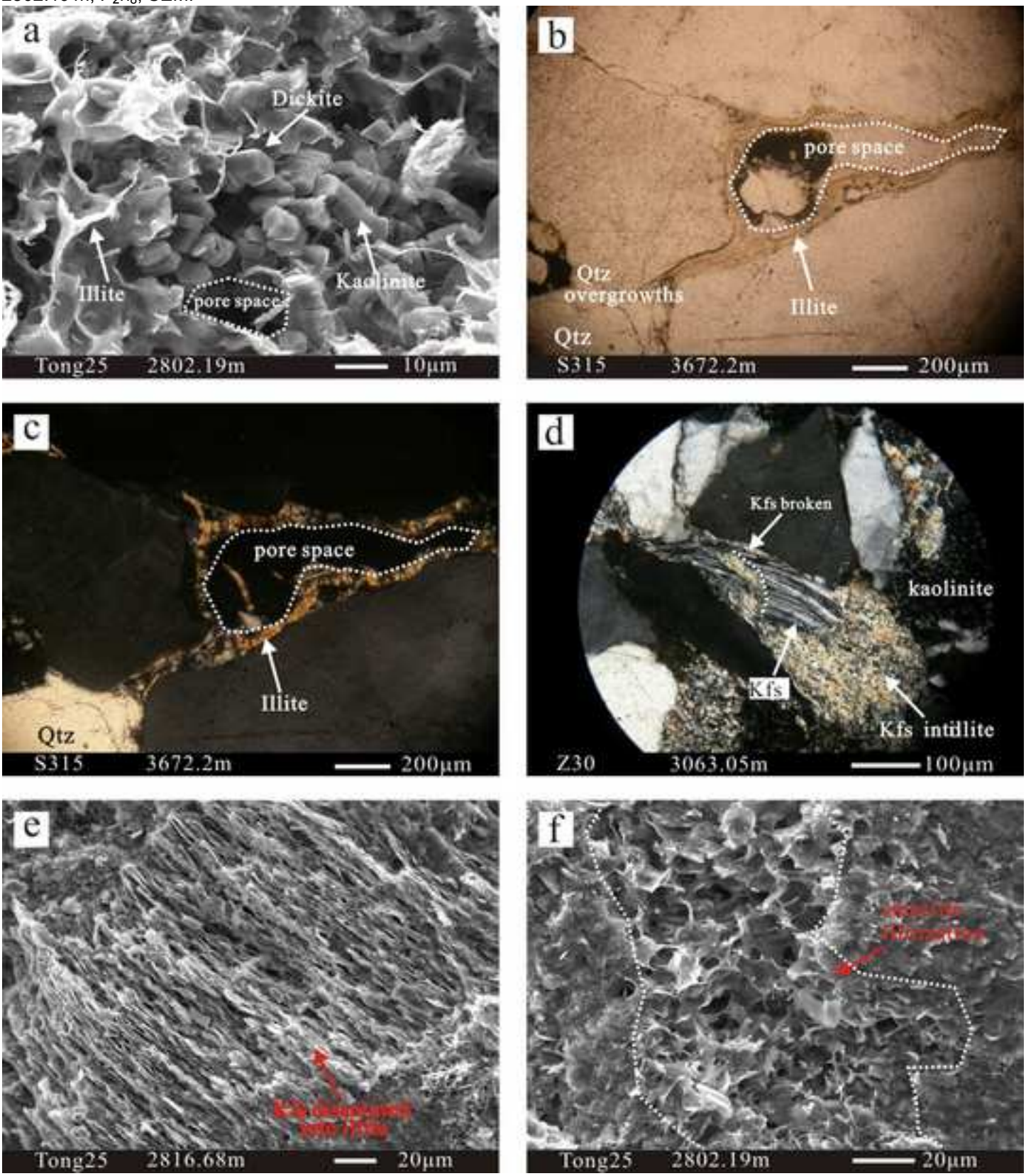

Figure-10. Thin section images of illite, kaolinite, kaolinite illitization, grain coating chlorite, chlorite replacing mica grains, pore-lining chlorite and quartz grains in the P_1s_1 and P_2h_8, Sulige Gas field. A. Kaolinite, illite and illitization of kaolinite, well S149, 3672.65 m, P_1s_1; B. grain coating chlorite, well S163, 2802.19 m, P_2h_8; C. chlorite replacing biotite, well S149, 3616.60 m, P_2h_8; D. pore-lining chlorite, well Z38, 3002.48 m, P_1s_1. Fig. 10A was taken under cross polarized light; B-D were taken under plane polarized light.

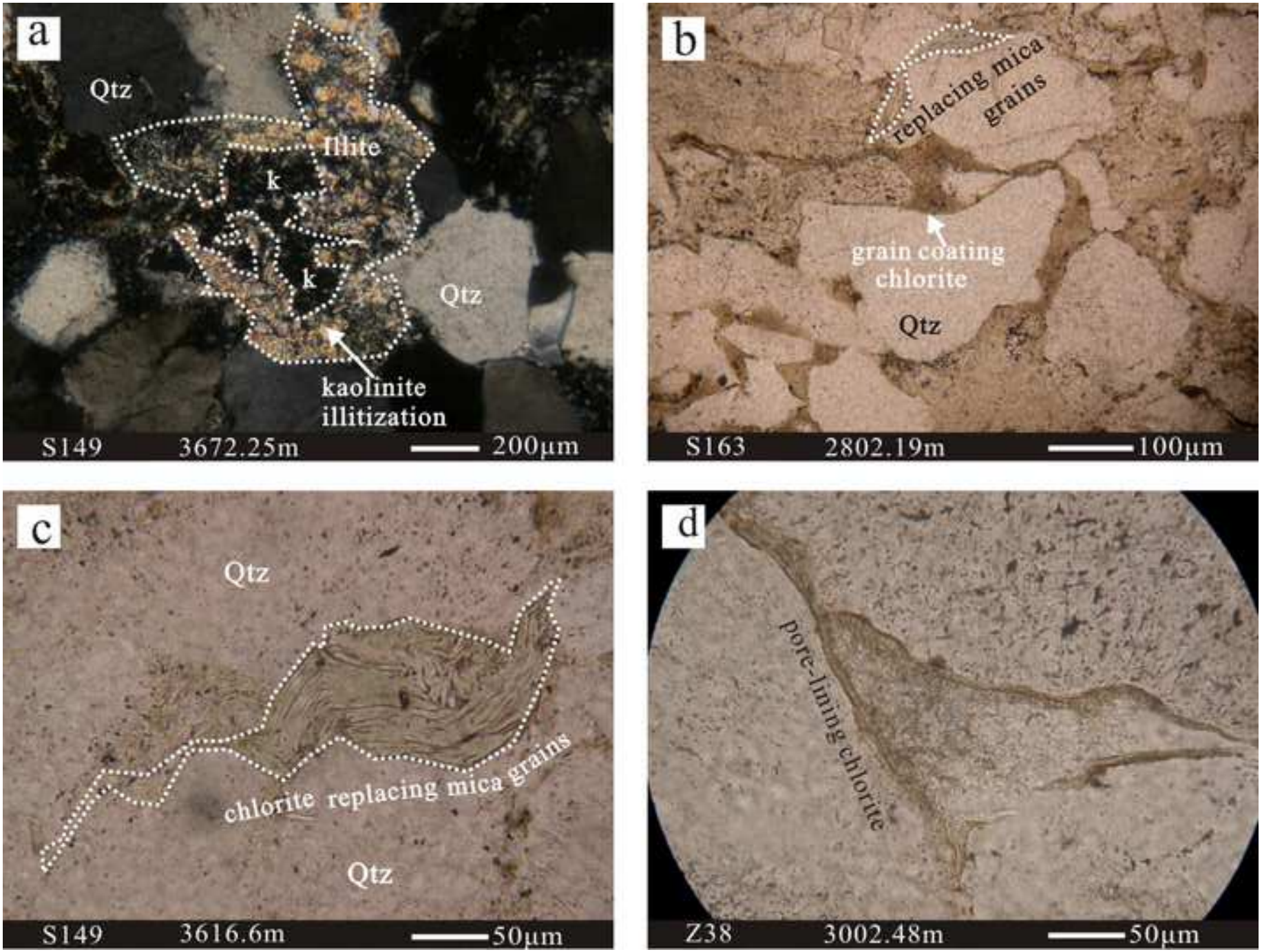

Figure-11. Quartz overgrowth, quartz outgrowth, illite and calcite cement of the sandstone reservoir, Sulige gas field. A. quartz overgrowth, well S315, 3671.40 m, P_2h_8; B. Illite, quartz outgrowth and pore space, well Tong 18, 3078.40 m, P_2h_8; C. calcite cement and replacement of kaolinite, well S47, 3587.95 m, P_2h_8; D. calcite cement and replacement of feldspar, well Z38, 3056.34 m, P_1s_1. Fig. 11A and C were taken under cross polarized light; B is an SEM image; D was taken under cathodoluminescence microscope.

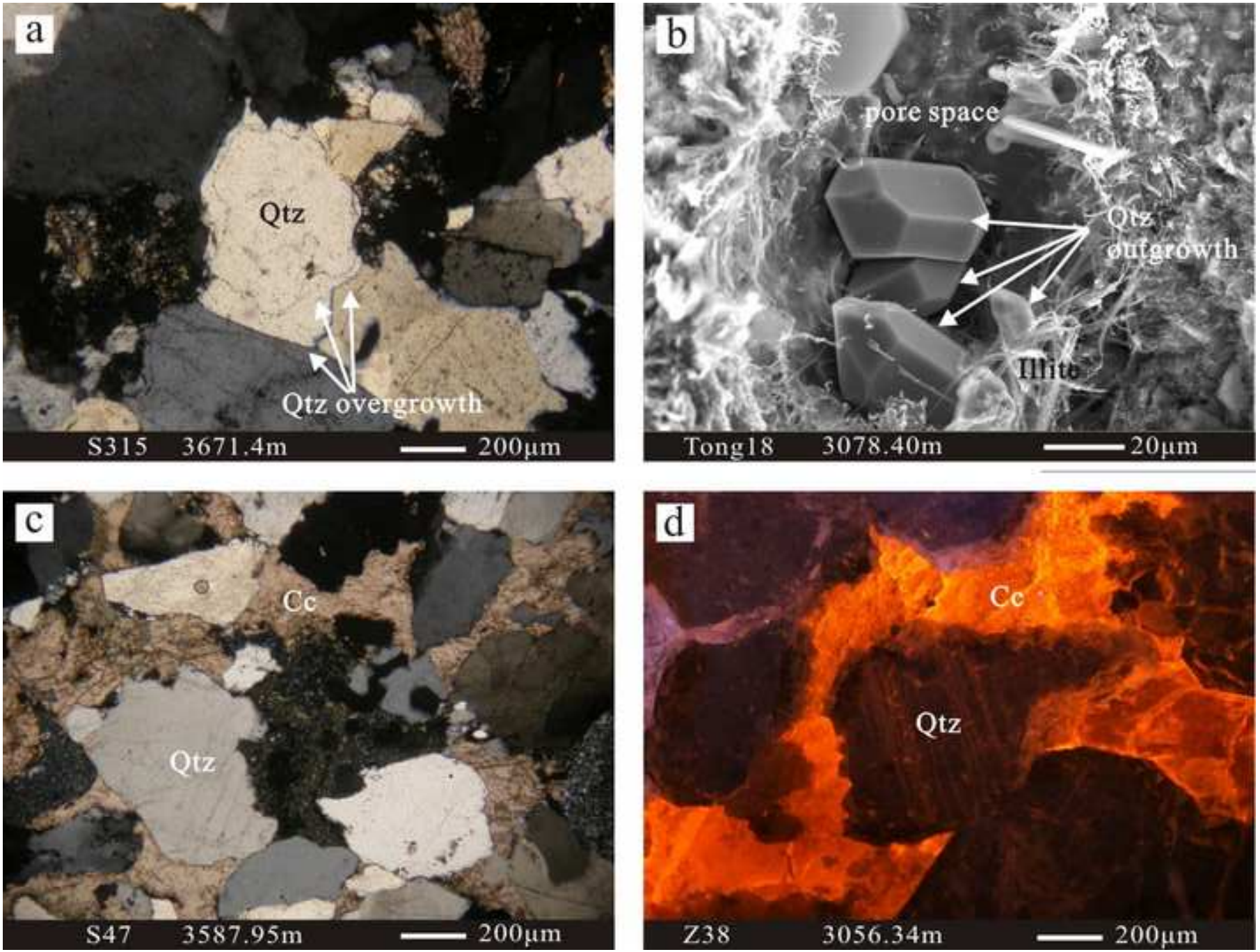

Figure-12. Three dimensional distribution of temperature measurements of homogeneous, freezing and initial melting temperature on diagenetic fluid inclusions in sandstone reservoirs, Sulige gas field.

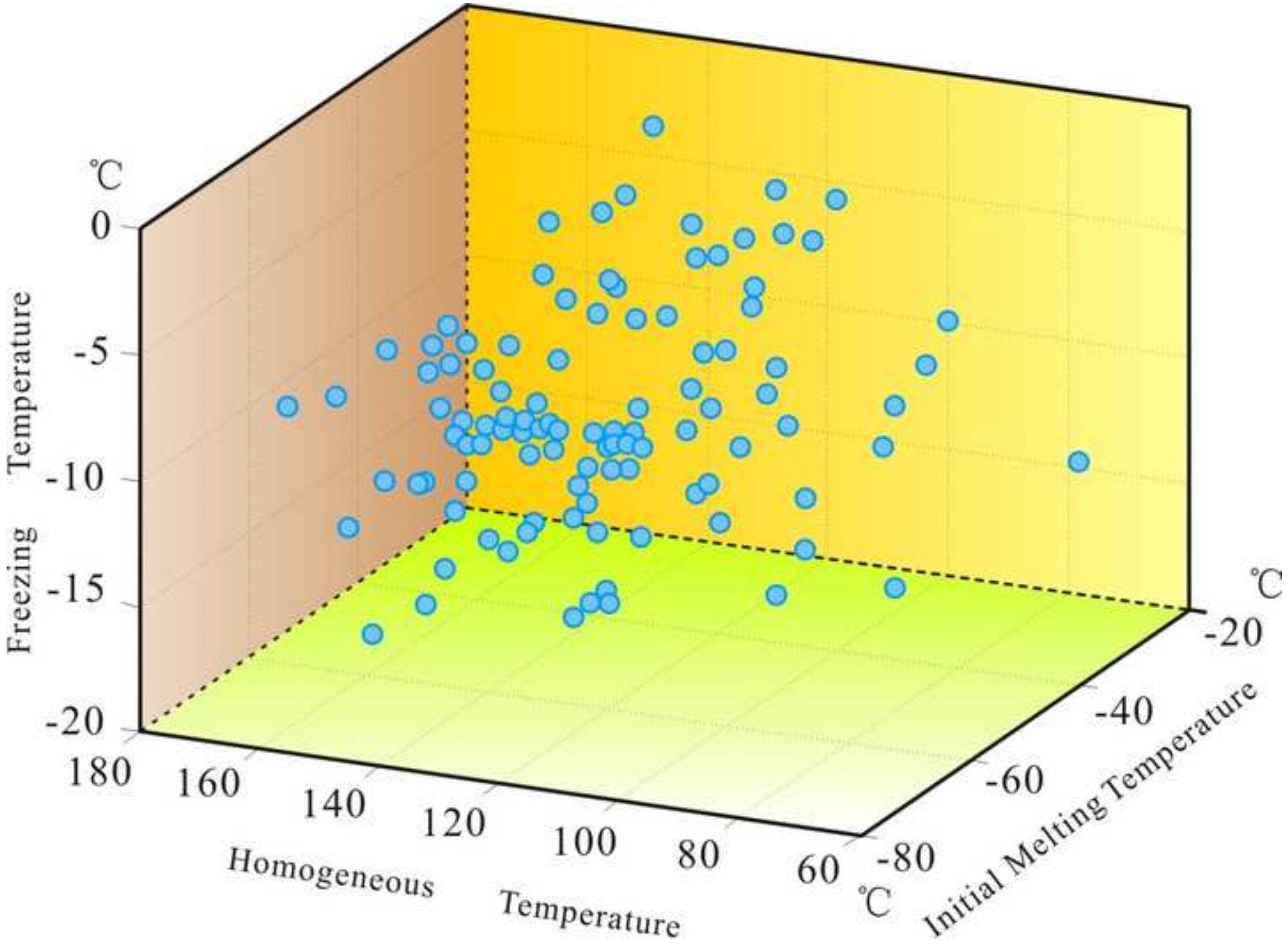

Figure-13. Correlation of porosity and sample depth in sandstone reservoirs, in the P1s1 and P2h8, Sulige gas field.

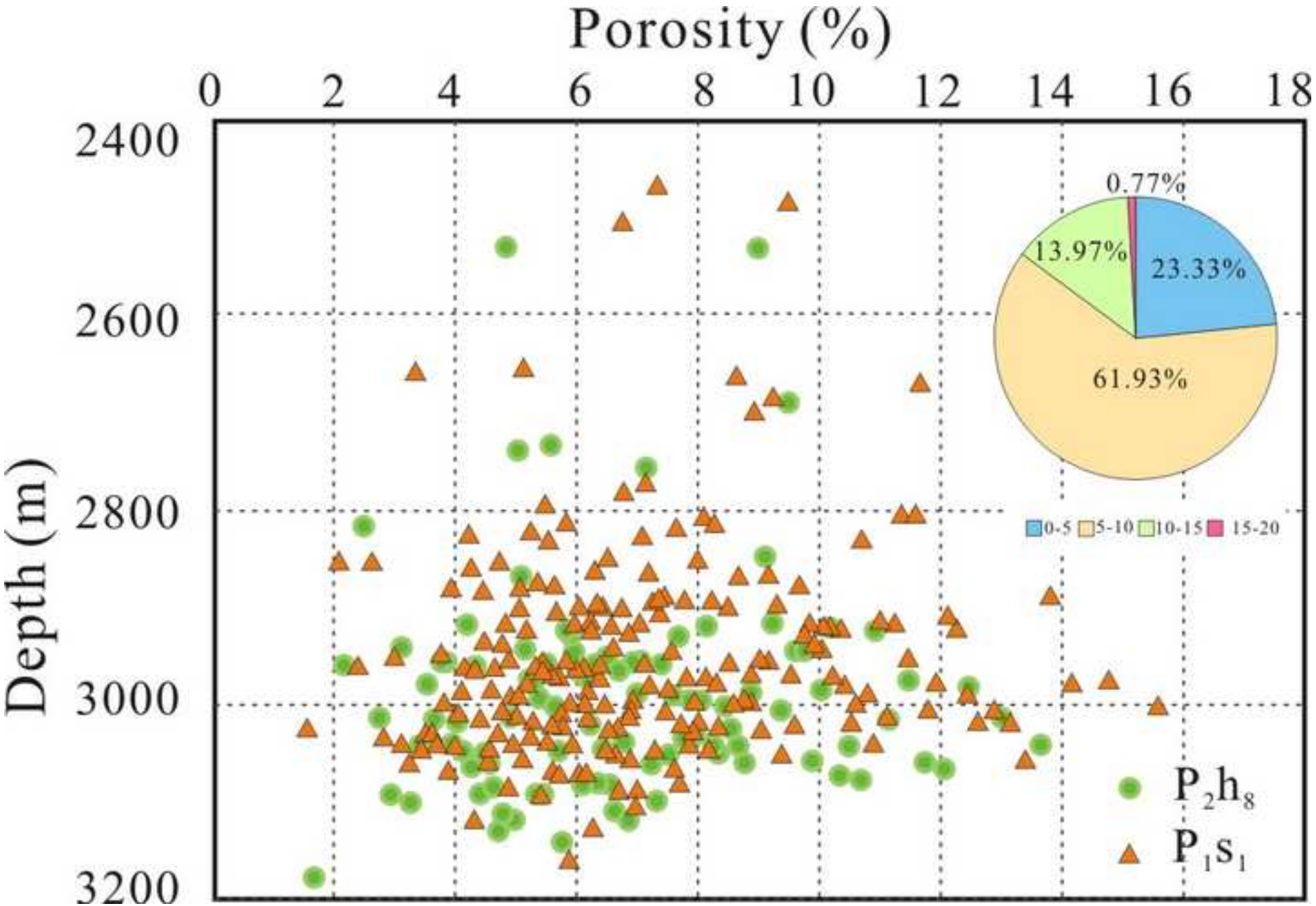

Figure-14. Types and ratios of pores in sandstone reservoirs, in the P_1s_1 and P_2h_8, Sulige gas field.

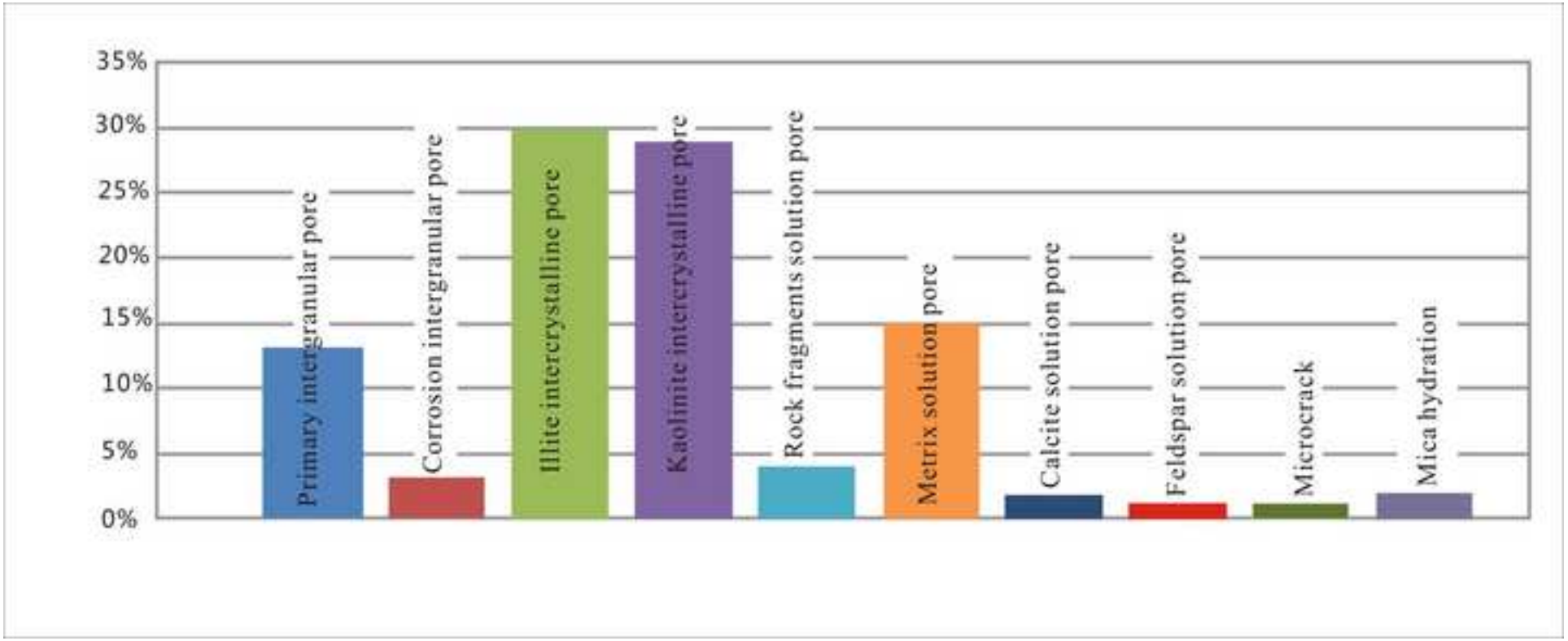

Figure-15. SEM images of kaolinite, chlorite rims, quartz outgrowth, illite, calcite and pores of the sandstone reservoir, Sulige gas field. A. kaolinite, chlorite rims and pores, well Zhao 14, 3027.19 m, P_2h_8; B. Kaolinite, quartz overgrowth and engulfing kaolinite in quartz overgrowth, well S174, 3663.75 m, P_2h_8; C. Illite, pores, and illite penetrating through kaolinite, well Tong 27, 2854.92 m, P_2h_8; D. Quartz and pore-filling of chlorite (after Fan et al., 2017), well Zhao 34, 3125.99 m, P_2h_8; E. Pore, chlorite and quartz engulfing chlorite, well Tong 32, 2705.06 m, P_1s_1; F. Illite and quartz outgrowth, well Yu149, 3050.13 m, P_2h_8; G. Pores, illite and quartz outgrowth, well Zhao 46, 3004.52 m, P_1s_1; H. Calcite, illite, quartz outgrowth and pores, well Yu149, 3050.13 m, P_1s_1.

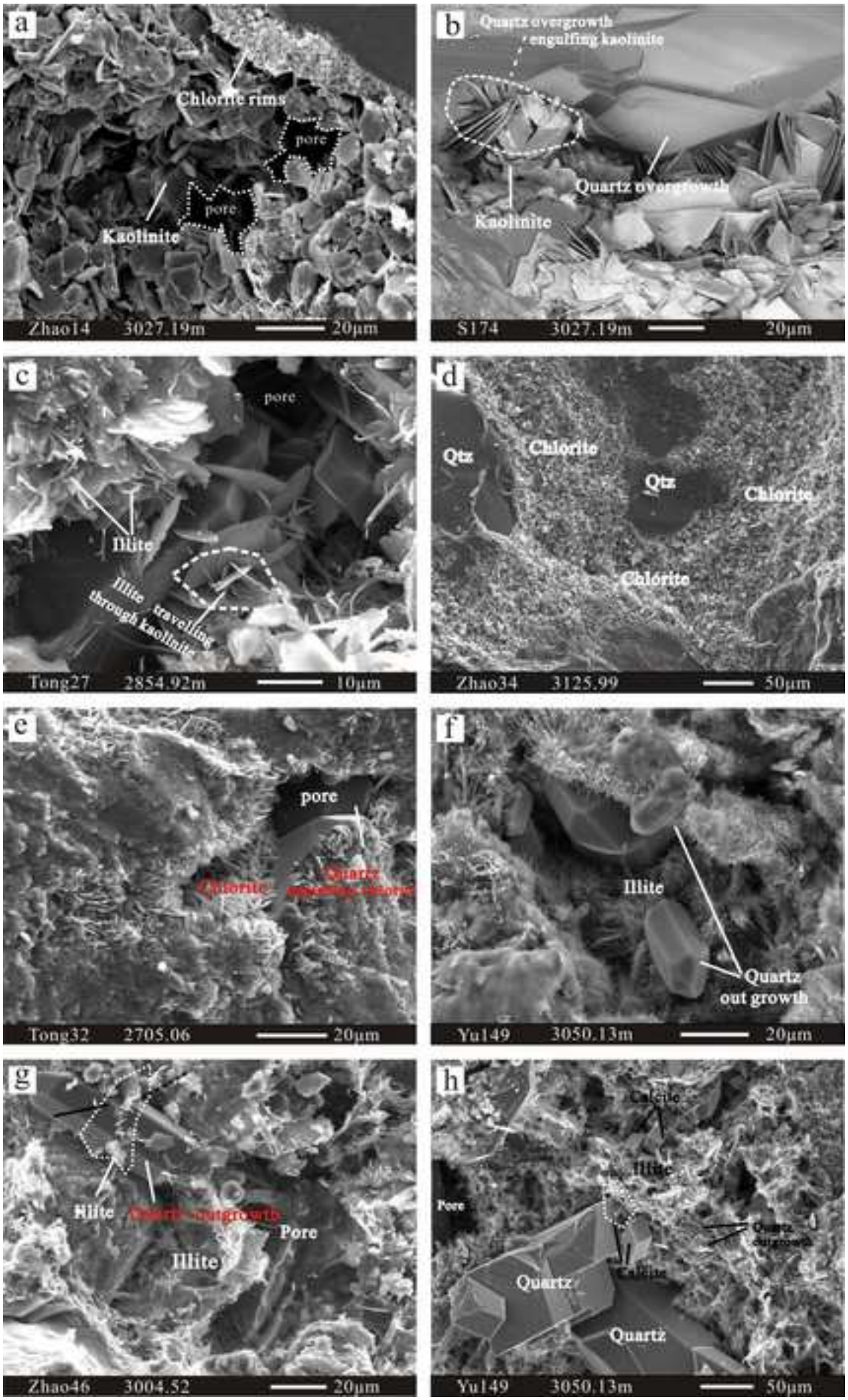

Table 1. Determination of homogenization temperature and salinity of two-phase brine inclusions

Well	Depth (m)	Occurrence	Initial melting Temperature (℃)			Homogeneous Temperature (℃)			Ice Point Temperature (℃)		
			Max	Min	Average	Max	Min	Average	Max	Min	Average
T29	2725.7	Fissure of quartz	-35	-50	-40.5	150	100	126.25	-3	-17	-8.5
T29	2725.7	Catenular inclusions	-30	-67	-48.9	169	115	138.6	-2	-13	-6.2
Z74	3032.3	Fissure of quartz	-79.5	-50.5	-60.77	151.3	65	123.13	-4	-18.3	-12
Z74	3032.3	Catenular inclusions	-35	-63	-51.4	170	100	124.8	-2	-19	-8
Z68	2803.04	Fissure of quartz	-37.2	-60	-51.7	152.4	113.1	131.6	-11.9	-6.8	-9.2
Z68	2803.04	Catenular inclusions	-39.4	-54.8	-46.6	123.3	93.2	107.8	-4.2	-11.8	-8.4
Z75	2887	Fissure of quartz	-42.1	-61.2	-54.6	158.2	120.5	133	-8.5	-15.3	-11.3
Z75	2887	Catenular inclusions	-36.8	-57.4	-48.8	131.6	63.2	98	-7.6	-16.3	-12.7
T29	2729.95	Fissure of quartz	-51.1	-65.6	-57.4	140.5	110	120.1	-8.9	-14.6	-10.6
Z52	2744.2	Fissure of quartz	-37.3	-67.5	-52.5	157.5	111.5	133.5	-3.7	-14.7	-9.4
Z46	2960	Fissure of quartz	-39.8	-69.5	-56.7	144	99.3	125.3	-3.2	-16.3	-10.4
Z39	2926.65	Fissure of quartz	-53	-79	-62.7	147.2	119.7	137	-5.1	-14.7	-9.6
Z38	3002.48	Quartz overgrowth	-17.9	-48.8	-33.4	148.4	125.5	137	-3.1	-10.3	-5.8
Z38	3009.42	Quartz overgrowth	-	-	-	87.3	87.3	87.3	3.2	3.2	3.2
Z38	3001.58	Quartz overgrowth	-	-	-	139.8	96.4	123.9	-2.1	-5.6	-3.5
Z30	3103.7	Quartz overgrowth	-	-	-	144.2	79.4	119.3	-2.1	-6.9	-4.2
Z30	3030.5	Calcite cement	-	-	-	188.6	170.3	179.8	-	-	-

Table 2. Physical properties of sandstone reservoirs in the Permian Sulige gas field

Strata	Sample number	Porosity (%)			Permeability (MD)		
		max	min	average	max	min	average
P_2h_8	227	18.64	3.98	9.57	4.595	0.11	0.576
P_1s_1	113	15.16	2.62	8.52	1.903	0.18	0.457